

JEVGENI ŠABLONIN

Processes of structural defect creation
in pure and doped MgO and NaCl
single crystals under condition
of low or super high density
of electronic excitations



JEVGENI ŠABLONIN

Processes of structural defect creation
in pure and doped MgO and NaCl
single crystals under condition
of low or super high density
of electronic excitations



This study was carried out at the Institute of Physics, University of Tartu, Estonia.

The dissertation was admitted on December 21, 2012, in partial fulfillment of the requirements for the degree of Doctor of Philosophy in physics (solid state physics) and allowed for defence by the Scientific Council of the Institute of Physics, University of Tartu.

Supervisors: Prof. Aleksandr Lushchik,
Institute of Physics, University of Tartu
Dr. Evgeni Vassil'chenko,
Institute of Physics, University of Tartu

Opponents: Dr. Anatoli Popov, Institute of Solid State Physics, Riga, Latvia

Defense: March 6, 2013 at University of Tartu, Tartu, Estonia

Publication of thesis was supported by: Graduate School on Functional Material and Technologies (GSFMT), University of Tartu.



ISSN 1406-0647
ISBN 978-9949-32-220-6 (print)
ISBN 978-9949-32-221-3 (pdf)

Copyright: Jevgeni Šablonin, 2013

University of Tartu Press
www.tyk.ee
Order No. 36

CONTENTS

LIST OF PUBLICATIONS.....	6
LIST OF ABBREVIATIONS	11
1. INTRODUCTION.....	12
2. EXPERIMENTAL	14
2.1. Objects.....	14
2.2. Methods and equipment.....	15
2.2.1. Photoluminescence.....	15
2.2.2. Cathodoluminescence.....	16
2.2.3. Thermostimulated luminescence.....	17
2.2.4. Optical absorption.....	17
3. THE MECHANISMS OF DEFECT CREATION	18
4. CRYSTAL STRUCTURE AND IMPERFECTIONS OF NaCl.....	20
4.1. A single crystal of NaCl.....	20
4.2. Intrinsic and impurity defects in NaCl.....	21
5. RESULTS OF EXPERIMENTS WITH NaCl.....	23
5.1. Non-impact defect creation at cryotemperatures.....	23
5.2. The Franck-Hertz effect as luminescent protection of NaCl:Ti ⁺	28
6. CRYSTAL STRUCTURE AND IMPERFECTIONS OF MgO.....	32
6.1. A single crystal of MgO.....	32
6.2. Intrinsic and impurity defects in MgO.....	34
6.3. Thermostimulated luminescence in MgO.....	37
7. RESULTS OF EXPERIMENTS WITH MgO.....	38
7.1 Impurity ions as luminescent protection against creation of FD.....	38
7.2. Bivacancies: charge carrier traps and the source of 2.9 eV emission.....	40
7.3. Localization of holes near impurities.....	42
7.4. The effect of swift heavy ions.....	47
7.5. Irradiation effects in MgO:Cr.....	49
SUMMARY	57
KOKKUVÕTE.....	61
AKNOWLEDGEMENTS.....	64
REFERENCES.....	65
PUBLICATIONS.....	69
CURRICULUM VITAE	141

LIST OF PUBLICATIONS

List of the original papers included in this thesis:

- I. A. Lushchik, Ch. Lushchik, T. Kärner, V. Nagirnyi, E. Shablonin, E. Vasil'chenko, "Impact and nonimpact creation mechanisms of radiation defects in ionic crystals", *Izvestija VUZOV. Fizika (Russian Physics Journal)* **52** (8/2), 95–100 (2009).
- II. A. Lushchik, Ch. Lushchik, T. Kärner, P. Liblik, V. Nagirnyi, E. Shablonin, A. Shugai, E. Vasil'chenko, "Franck-Hertz effect in cathodo- and photoluminescence of wide-gap materials", *Radiation Measurements* **45**, 268–272 (2010).
- III. S. Dolgov, T. Kärner, A. Lushchik, A. Maaros, S. Nakonechnyi, E. Shablonin "Trapped-hole centers in MgO single crystals", *Phys. Solid State*, **53** (6), 1244–1252 (2011) [*С.А. Долгов, Т. Кярнер, А. Луццик, А. Маароос, С. Наконечный, Е. Шаблонин, "Локализованные дырки в монокристаллах MgO", ФТТ, т. 53 (6), сс. 1179–1187 (2011)]*.
- IV. A. Lushchik, Ch. Lushchik, I. Kudryavtseva, A. Maaros, F. Savikhin, E. Shablonin, E. Vasil'chenko, "Low-temperature investigation of electronic excitations in wide-gap materials doped with RE³⁺ and Cr³⁺ impurity ions", *Optics and Spectroscopy* **111** (3), 434–440 (2011) [*Низкотемпературное исследование электронных возбуждений в широкощелевых материалах, легированных ионами RE³⁺ или Cr³⁺, Оптика и спектроскопия III(3), 458–465 (2011)]*.
- V. A. Lushchik, Ch. Lushchik, K. Schwartz, F. Savikhin, E. Shablonin, A. Shugai, E. Vasil'chenko, "Creation and clustering of Frenkel defects at high density of electronic excitations in wide-gap materials," *Nucl. Instr. and Meth. B* **277**, 40–44 (2012).
- VI. A. Lushchik, T. Kärner, Ch. Lushchik, K. Schwartz, F. Savikhin, E. Shablonin, A. Shugai, E. Vasil'chenko, "Electronic excitations and defect creation in wide-gap MgO and Lu₃Al₅O₁₂ crystals irradiated with swift heavy ions", *Nucl. Instr. and Meth. B* **286**, 200–208 (2012).
- VII. A. Lushchik, Ch. Lushchik, V. Nagirnyi, S. Pazylybek, O. Sidletskiy, K. Schwartz, E. Shablonin, A. Shugai, and E. Vasil'chenko, "On the mechanisms of radiation damage and prospects of their suppression in complex metal oxides", *Physica Status Solidi B* **250**, 261–270 (2013).

The author's contribution to publications:

The papers that form the basis for the thesis are the result of a collective work with an important contribution by all the coauthors. The author has given an essential input to all the publications; his contribution to the papers can be described as follows:

- Publication I: CL and PL spectra measurements, processing and analysis of experimental data on NaCl and MgO, preparation of figures, participation in writing of the manuscript.
- Publication II: Obtaining, processing and analysis of experimental data on MgO. Participation in the elaboration of the general concept, preparation of figures, writing of the manuscript.
- Publication III: Obtaining of the experimental data on Ca-related trapped-hole centers, processing and analysis of data, participation in writing of the corresponding part of the manuscript.
- Publication IV: Obtaining, processing and analysis of experimental data on Cr³⁺ impurity centers in MgO, participation in writing of the corresponding part of the manuscript.
- Publication V: Obtaining, processing and analysis of experimental data related to MgO. Participation in the elaboration of the general concept, preparation of figures, writing of the manuscript.
- Publication VI: The main author of the section "Radiation effects in MgO single crystals".
- Publication VII: Obtaining, processing and analysis of experimental data on radiation effects in MgO. Participation in the elaboration of the general concept, preparation of figures and participation in writing of the corresponding part of the manuscript.

Other publications:

- VIII. A. Baimakhanuly, E. Vasil'chenko, Ju. Maksimov, L. Pung, E. Shablonin, "The role of electronic excitations in the creation of nano-size defects in KCl", *Izv.VUZOV, Fizika (Russian Physics Journal)* **52**, N 8/2, 18–21 (2009).
- IX. S. Dolgov, A. Kotlov, I. Kudryavtseva, A. Lushchik, V. Nagirnyi, E. Shablonin, E. Vasil'chenko, "Creation spectra of F centres by 7–40 eV photons in NaCl crystals at 300 or 12 K", In: *MAX-LAB Activity Report 2008*, National Laboratory, Lund, Sweden, 96–97 (2009).
- X. A. Lushchik, V. Nagirnyi, E. Shablonin, O. Sidletskiy, B. Toxanbayev and A. Zhunusbekov, "Luminescence of cation excitons in Gd₂SiO₅ crystals", In: *HASYLAB Activity Report 2009, Part I*, DESY, Hamburg, Germany (2009).

- XI. A. Lushchik, S. Dolgov, I. Kudryavtseva, T. Kärner, F. Savikhin, E. Vasil'chenko, E. Shablonin, A. Shugai, "Attenuation of radiation damage in dielectric and composite materials of interest for a fusion reactor", *Fusion Yearbook Association Euratom-Tekes, Annual Report 2009*, VTT Publications 7389, Helsinki, Finland, 69–72 (2010).
- XII. E. Feldbach, A. Lushchik, Ch. Lushchik, V. Nagirnyj, E. Shablonin, S. Vielhauer, "Creation of long-lived Frenkel defects via hot electron-hole recombination in pure NaCl crystals at 12 K", in: *MAX-LAB Activity Report 2010*, National Laboratory, Lund, Sweden, 462–463 (2010).
- XIII. S. Dolgov, T. Kärner, A. Lushchik, E. Shablonin, "Recombination of conduction electrons with trapped-hole centres in MgO:Be and MgO:Ca single crystals", *Bulletin of Karaganda University (Вестник Карагандинского университета)* **1** (61), 15–20 (2011).
- XIV. A. Lushchik, V. Nagirnyj, K. Schwartz, E. Shablonin, A. Shugai, "Electronic Excitations and Defect Creation in $\text{Lu}_3\text{Al}_5\text{O}_{12}$ Crystals Irradiated with Swift Heavy Ions", In: *HASYLAB Activity Report 2011*, DESY, Hamburg, Germany, 2 pages in the online version (2012).

List of conferences:

- I. A. Baimakhanov, A. Kotlov, I. Kudryavtseva, A. Lushchik, V. Nagirnyi, E. Shablonin, E. Vasil'chenko, "Peculiarities of radiative and non-radiative decay channels of intrinsic electronic excitations in NaCl", *International Baltic Sea Region conference "Functional materials and nanotechnologies,"* Riga, April 1–4, Po-10 (2008) (poster).
- II. E. Shablonin, T. Kärner, P. Liblik, A. Lushchik, A. Maaros, V. Nagirnyi, F. Savikhin, E. Vasil'chenko, "Electron and hole processes in MgO crystals", *International Baltic Sea Region Conference "Functional materials and nanotechnologies,"* Riga, March 31–April 3, Po-23 (2009) (poster).
- III. A. Lushchik, Ch. Lushchik, T. Kärner, P. Liblik, V. Nagirnyi, E. Shablonin, A. Shugai, E. Vasil'chenko, "Franck-Hertz effect in cathodo- and photoluminescence of wide-gap materials", *7th International Conference on Luminescent Detectors and Transformers of Ionizing Radiation*, Krakow, Poland, July 12–17, Mo-7 (2009) (invited lecture).
- IV. A. Lushchik, Ch. Lushchik, T. Kärner, V. Nagirnyi, E. Shablonin, and E. Vasil'chenko, "Impact and nonimpact creation mechanisms of radiation defects in ionic crystals", *14th International Conference on Radiation Physics and Chemistry of Inorganic Materials (RPC-14)*, Astana, Kazakhstan, October 6–10 (2009) (invited lecture).
- V. A. Baimakhanuly, E. Vasil'chenko, Ju. Maksimov, L. Pung, E. Shablonin, "The role of electronic excitations in the creation of nano-size defects in KCl", *14th International Conference on Radiation Physics and*

- Chemistry of Inorganic Materials (RPC-14)*, Astana, Kazakhstan, October 6–10 (2009) (oral).
- VI. E. Shablonin, “Luminescent protection against the creation of Frenkel defects at the irradiation of NaCl and MgO single crystals by VUV radiation, electrons and swift ions”, *TÜ ja TTÜ doktorikooli “Funktsionaalsed materjalid ja tehnoloogiad” esimene teaduskonverents*, Tartu, Estonia, February 25–26 (2010) (poster).
 - VII. E. Shablonin, T. Kärner, A. Lushchik, K. Schwartz, E. Vasil’chenko, “Impact and nonimpact creation of defects in MgO crystals under swift-heavy-ion-irradiation”, *11th Europhysical Conference on Defects in Insulating Materials (EURODIM 2010)*, Pecs, Hungary, July 12–16 (2010) (poster).
 - VIII. A. Lushchik, A. Baimakhanuly, A. Kotlov, V. Nagirnyi, E. Shablonin, E. Vasil’chenko, “Defect creation via hot carriers recombination or decay of cation excitons in NaCl and MgO at 6–12 K”, *Abstr. 11th Europhysical Conference on Defects in Insulating Materials (EURODIM 2010)*, Pecs, Hungary, July 12–16 (2010) (oral talk).
 - IX. Ch. Lushchik, I. Kudryavtseva, T. Kärner, A. Lushchik, F. Savikhin, E. Shablonin, E. Vasil’chenko, “Low-temperature study of intrinsic electronic excitations in wide-gap materials using luminescent RE³⁺ and Cr³⁺ impurity ions”, *XIV International Feofilov Symposium on Spectroscopy of Crystals Doped with Rare Earth and Transition Metal Ions*, St. Petersburg, October 18–21 (2010) (oral talk).
 - X. E. Shablonin, “Radiation-induced defects in MgO crystals under swift-heavy-ion-irradiation”, *TÜ ja TTÜ doktorikooli “Funktsionaalsed materjalid ja tehnoloogiad” teine teaduskonverents*, Tallinn, Estonia, March 3–4 (2011) (poster).
 - XII. A. Lushchik, Ch. Lushchik, K. Schwartz, F. Savikhin, E. Shablonin, A. Shugai, E. Vasil’chenko, “Creation and clustering of Frenkel defects at high density of electronic excitations in wide-gap materials”, *EMRS 2011 Spring Meeting, Symposium L “Basic research on ionic-covalent materials for nuclear applications”*, Nice, France, May 9–13, L3–5 (2011) (oral talk).
 - XIII. A. Lushchik, Ch. Lushchik, K. Schwartz, F. Savikhin, E. Shablonin, A. Shugai, E. Vasil’chenko, “Contribution of electronic excitations to defect creation in wide-gap metal oxides irradiated with swift heavy ions or fast electrons”, *16th International Conference on Radiation Effects in Insulators (REI-2011)*, Beijing, China, August 14–19, I-1, Abstr. p. 34 (2011) (invited lecture).
 - XIV. E. Shablonin, “Electronic Excitations and Defect Creation in Wide-gap MgO Single Crystals Irradiated with Swift Heavy Ions”, *TÜ ja TTÜ doktorikooli “Funktsionaalsed materjalid ja tehnoloogiad” kolmas teaduskonverents*, Tartu, Estonia, February 29–March 1 (2012) (poster).

- XV. A. Luschik, Ch. Lushchik, V. Nagirnyj, S. Pazyzbek, O. Sidletskiy, K. Schwartz, E. Shablonin, A. Shugai, E. Vasil'chenko, "On the nonimpact mechanisms of radiation damage and prospects of their suppression in complex metal oxides", *International Conference on Defects in Insulating Materials (ICDIM 2012)*, Santa Fe, USA, June 25–29 (2012) (oral talk).

LIST OF ABBREVIATIONS

Abs.	optical absorption
β	heating rate
CL	cathodoluminescence
e	electron
$e-h$	electron-hole
EE	electronic excitations
E_{FD}	formation energy of a Frenkel defect
E_g	band gap
E_i	ionization energy
E_{kin}	kinetic energy
EPR	electron paramagnetic resonance
fcc	face-centered cubic
FD	Frenkel defects
SSAFHE	solid-state analogue of the Franck-Hertz effect
h	hole
$h\nu$	photon energy
IR	infrared
LET	linear energy transfer
OD	optical density
PL	photoluminescence
PMT	photomultiplier tube
PSL	photostimulated luminescence
RPCC	rhombic pair chromium center
RT	room temperature
r_a, r_c	anion radius, cation radius
TSL	thermostimulated luminescence
SHI	swift heavy ions
SR	synchrotron radiation
STE	self-trapped exciton
UV, VUV	ultraviolet, vacuum ultraviolet
v_a, v_c	anion vacancy, cation vacancy
WGM	wide-gap materials

I. INTRODUCTION

Wide-gap materials (WGM, $E_g = 5\text{--}15$ eV) are widely used for many technical applications as fast scintillation detectors, laser hosts, spectral transformers in mercury-free fluorescence lamps and displays, materials for optical components, safety inspection systems and nuclear energetics, dosimeters for medical and industrial purposes, etc. Under operating conditions, WGM suffer the influence of different types of radiation: vacuum-ultraviolet (VUV) light, X- and γ -rays, electrons, protons, fast neutrons, swift heavy ions (SHI), etc. Therefore, among many specific requirements, a sufficient resistance of WGM against different types of radiation under operating conditions is of particular importance. In particular, the success in future industrial thermonuclear (fusion) reactors cannot be achieved without a significant increase in the radiation resistance of construction and diagnostics materials.

Many WGM, such as most alkali halides, are rather susceptible to ionizing radiation, because the formation energy of a pair of Frenkel defects (FD) in these materials is smaller than the energy gap ($E_{\text{FD}} < E_g$) [1–4]. However, the minimization of the creation efficiency of radiation-induced nano- and micro-size defects, as well as their thermal annealing (for repeated use of functional materials) is relatively easy to perform in WGM, where $E_{\text{FD}} > E_g$. In such WGM, the energy released at the recombination of relaxed electrons (down to the bottom of a conduction band) and holes (up to the top of a valence band) is insufficient for the creation of FD (vacancies and interstitials).

The general goal of our study was to continue the investigation of the processes of radiation defects creation in pure and doped MgO [5, 6] and NaCl single crystals – representatives of two groups of binary WGM with the same face centered cubic type of crystalline lattice, close values of E_g (7.8 and 8.75 eV, respectively), but rather different levels of radiation resistance. In radiation-resistant MgO, the inequality $E_{\text{FD}} > 3E_g$ is valid in the whole temperature range, while in NaCl $E_{\text{FD}} > E_g$ only at low temperatures, $T < 120$ K. In NaCl at room temperature (RT), expansion of crystalline lattice results in a decreasing value of E_{FD} . As a result, at high temperatures $E_{\text{FD}} < E_g$, and NaCl belongs, like a majority of alkali halide crystals (e.g., KCl) in the whole temperature range, to radiation-sensitive WGM.

It was suggested, that hot electron-hole ($e\text{--}h$) recombination could be responsible for the creation of elementary FD in NaCl at $T < 120$ K. In the framework of the doctoral study, we planned to confirm this hypothesis as well as to analyze the prospects for the suppression of hot $e\text{--}h$ recombination via a solid-state analogue of the Franck-Hertz effect (SSAFHE) in NaCl doped with luminescent impurity ions. Particular attention has been paid also to the influence of divalent (i.e. isovalent Be^{2+} , Ca^{2+}) and trivalent impurity ions (Al^{3+} , Fe^{3+} , Cr^{3+} , charge compensation is needed) on the efficiency of radiation damage in high-refractory MgO single crystals (melting point at ~ 3200 K) grown at the Institute of Physics by a variation of the arc-fusion method.

A new challenge has been to investigate the peculiarities of the creation processes of FD, their simple and more complex associations in highly pure or doped with certain impurity ions MgO single crystals under irradiation with SHI. Besides the knock-out (impact) mechanism connected with elastic collisions of incident particles with the atoms of a crystals providing the formation of FD and more complex defects, SHI (^{198}Au , ^{238}U , energy of ~ 2 GeV) spent more than 99% of their energy on the ionization and excitation of an electron subsystem resulting in an extremely high density of electronic excitations (EE, linear energy transfer $\text{LET} > 20$ keV/nm). The efficient creation of complex defects covering both anion and cation sublattices via a joint action of an impact and nonimpact mechanism is expected under such irradiation of binary MgO crystals. According to theorists, one might also expect the creation of 3D defects – rearrangement of many host ions in the vicinity of heavy impurity ions, caused by ultrasonic impact waves [7–9]. In MgO, close pairs of Cr^{3+} – Cr^{3+} can tentatively serve as seeds for this type of 3D defect creation.

This thesis is based on the experimental results that have been published in the works presented for this PhD viva [I–VII]. Most of the experimental results in this work have been obtained in the Laboratory of Physics of Ionic Crystals at the Institute of Physics, University of Tartu, and at SUPERLUMI station in HASYLAB, DESY, Germany.

2. EXPERIMENTAL

2.1. Objects

The single crystals of NaCl used in this study had different origin:

1. A crystal grown at the Institute of Physics, Tartu University, from a specially purified and dried (to remove OH^- ions) starting material by the Kyropoulos method in inert He atmosphere. A NaCl melt was preliminarily treated with a Cl_2 flow to remove Br^- and I^- . The purified starting material was placed into an ampoule made from highly pure quartz and then subjected to a 40-fold zone melting to lower the concentration of metallic impurities. This crystal will be referred to as “highly pure”.
2. A highly pure natural crystal (hereinafter referred to as “natural”), which has grown from a solution under natural conditions at temperatures close to RT. Such conditions provide a slower growth speed than growth from the melt, but the surface density of dislocation is lower ($\leq 3 \times 10^4 \text{ cm}^{-2}$), and distribution coefficients for all impurities (including Ca^{2+}) are also smaller, so the resultant crystals are purer: the estimated concentration of Ca^{2+} ions was several ppm. The concentration of OH^- ions was examined optically up to 7.4 eV and found to be negligible. So, natural crystals were less contaminated and structurally more perfect than artificial samples.
3. Crystals produced (in 2000) by Leitz company via growing from melt in an inert atmosphere. The main impurities in these crystals (which will be referred to as “NaCl (Leitz)”) were K^+ , Ca^{2+} , and Br^- .

MgO crystals – both pure and doped with Ca^{2+} (~200 ppm), Be^{2+} (~150 ppm), Cr^{3+} (100 or 850 ppm) or Al^{3+} – were grown by A. Maaros in the Laboratory of Ionic Crystals of the Institute of Physics, University of Tartu, by a variation of the arc fusion technique, wherein the walls of the growth container are of the same material as the crystals being grown, preventing contamination and serving as seed crystals. This growth technique, which allows obtaining MgO crystals with a size of up to $1,5 \times 1,5 \times 1 \text{ cm}^3$, is based on modified Stöber’s method [10] in combination with other methods [11, 12] of single crystals growth. The melting temperature of MgO was achieved with a two-electrode arc furnace (current 250–300 A). The starting material was magnesium oxide with a purity of 99.99% “oc.ч. 11–2” or “Alfa Aesar”. To decrease the concentration of impurities, the crystals grown from this material were used as the starting material for the second growth. Dopants of grade “oc.ч.” or “Alfa Aesar” (99.99% pure in both cases) were added to the starting material as CaCO_3 in the case of Ca^{2+} -doping or as respective oxides in the case of other metallic ions. The starting material was preliminarily compressed into blocks under a pressure of 290 kg/cm^2 . A detailed description of the growth method has been published in [13]. The concentration of impurities in the grown crystals was determined by chemical analysis or EPR methods.

To produce defects, the crystals were irradiated by UV and VUV photons (4–40 eV, synchrotron radiation), X-rays (50 kV, 15 mA), excimer lasers in the two-photon absorption mode (KrF-laser: $4.99 \times 2 = 9.98$ eV, ArF-laser: $6.42 \times 2 = 12.84$ eV, EXCIMER LASER PSX-100), an electron beam (5–15 keV), or swift heavy ions (^{238}U , ^{196}Au , 1–2 MeV, 50 Hz-impulses of 0.1–5 ms; irradiation was carried out at UNILAC, Darmstadt, Germany by K. Schwartz).

2.2. Methods and equipment

Due to the complexity of the processes connected with interactions between a variety of defects (as-grown and radiational) and ionizing radiation, it is necessary to use different research methods that complement each other. In this work, information about objects was obtained using photoluminescence (PL), cathodoluminescence (CL), photostimulated luminescence (PSL), thermally stimulated luminescence (TSL), and optical absorption (Abs). Luminescent techniques have the advantage of being easy, fast, nondestructive, and having a relatively high sensitivity, which allows studying defects with concentrations in the order of several ppm.

2.2.1. Photoluminescence

PL and PSL measurements were mainly conducted using synchrotron radiation (SR) at SUPERLUMI station (DESY, Hamburg, Germany), but some experiments were also made at undulator beamline I3 of MAX-III in MAX-Lab (Lund, Sweden).

SUPERLUMI experimental setup [14] is optimized for selective excitation in the VUV spectral range ($h\nu \leq 40$ eV) and for luminescence analysis from the VUV to the near IR range. The pulsed nature of SR and a chopper enable time resolution in the range of ps to ms.

The setup includes a primary monochromator for excitation and three secondary monochromators for luminescence analysis. The primary monochromator has focal length of 2 m, covers the spectral range from ~ 4 to 40 eV, and in our experiments the 30 μm wide entrance slit was used. Secondary monochromators include the Pouey monochromator (not used by us), the VUV monochromator (used in some rare cases), and the usually used 0.3 m monochromator in Czerny-Turner mounting (three gratings 300/600/1200 grooves per mm). This main instrument has two exit arms. One of them serves a liquid nitrogen cooled CCD detector; the other one serves a fast photomultiplier (for time-resolved experiments). The practical limit of spectral resolution (with 1200 grooves per mm grating) is $\Delta\lambda = 0.15$ nm. The working range is 200 nm to 1 μm .

The incident angle of synchrotron beam onto an object is 17° – close to normal, and the light spot has a rectangular shape of about 3×1 mm².

The liquid helium flow cryostat allows conducting experiments in the temperature range from RT to 8–9 K. In this work, all the synchrotron measurements were made at the lowest temperatures.

The working region (4–40 eV) of the primary monochromator is covered by two gratings: Al-grating (used for the 4–20 eV region) and Pt-grating (for the 15–40 eV region). Each grating has different efficiency distributions, hence, all spectra have to be corrected before analysis. Additionally, for the Al-grating two filters are used to eliminate excitation by the second orders of grating: a quartz filter for the energies below 7 eV and a MgF₂ filter for energies 7–9 eV. Due to absorption, the MgF₂ filter severely cuts the intensity of excitation, considerably reducing the signal to noise ratio. The signal is also weakened in the region of 17–20 eV due to the grating inefficiency, which sometimes makes it completely impossible to register anything besides noise. The same difficulty arises in the 36–40 eV region of the Pt-grating. Also, there is a gradual decrease over time in the current of synchrotron and, therefore, in the overall intensity of synchrotron radiation between injections. All of these factors have to be taken into account, and the original spectra need to be corrected accordingly.

The sensitivity distributions of CCD and PMT detectors were not available, so no respective corrections had been done.

2.2.2. Cathodoluminescence

The CL spectra were measured with a custom-made two-channel setup, which allowed registering luminescence in the region of 1.8–11 eV at temperatures 5–430 K. In this setup, excitation is carried out with an electron gun (1–30 keV, 10 nA–5 μ A). An electron beam is focused on the surface of an object into a spot of about 0.5 mm², with the penetration depth of electrons being \sim 0.5 μ m and \sim 1 μ m for energies 5 and 10 keV, respectively. A typical thickness of an object is 0.5–1 mm. The short-wavelength channel (4–11 eV) has a Johnson–Onaka vacuum double monochromator (with a grating for the dispersive element, $\Delta\lambda = 0.167$ nm/mm) and a R6838 photomultiplier. The channel for longer wavelengths (1.7–6.0 eV) had a double prism monochromator and a photon counter Hamamatsu H6240. After irradiation, the phosphorescence or thermostimulated luminescence of a selected energy can be registered in both channels. Additionally, integral thermostimulated luminescence in the region of 1.8–6.0 eV can be registered, if the short-wavelength channel is replaced with an external detector, which is mounted onto the object window of the cryostat.

In the case of dielectric objects, the problem of surface charges arises. Those charges cause flashes, revealing in the CL spectra as random peaks. To avoid or at least suppress this effect, either conductive surface coatings or low beam energies and currents have to be used. In this work, we usually resorted to the second option, using 5 keV and 100 nA beams, but in some cases objects coated with a \sim 9 nm layer of gold were also used, which allowed working with electron energies of 10–15 eV and currents 100–300 nA.

2.2.3. Thermostimulated luminescence

The TSL spectra were measured from 5 K to 823 K with two instruments. The first one, covering the interval of 5–420 K with the heating rate $\beta = 10$ K/min, has already been described in the previous section.

The other one used for registering high-temperature TSL from room temperature up to 823 K with $\beta = 2$ K/s was a Harshaw 3500 TLD Reader. Luminescence is registered with a cooled Hamamatsu photomultiplier tube, and a sample is kept in a nitrogen flow. The default detection region is 1.9–4.1 eV (according to the PMT specifications), but it can be narrowed by replacing a white glass filter with a colored one.

At temperatures above ~ 780 K, it is complicated to measure TSL due to the increasing level of heater glow. At 800 K and higher temperatures, the intensity of this red glow in many cases is comparable to the TSL signal intensity or even exceeds it. To remove this background, after the initial measurement of an irradiated crystal we measured the same object for the second time and separated the TSL signal by subtracting the second curve from the first one. However, the heater performance above 800 K is not stable, which leads to deviations from linearity and differences in the intensities of spectra measured under the same conditions. These differences may appear in differential spectra as a positive or negative exponential growth of a signal at the end of a spectrum, which must be taken into account during spectra analysis.

2.2.4. Optical absorption

Optical absorption was measured with a spectrophotometer Jasco V-550, which is able to register absorption or transmission spectra in the region 900–190 nm (1.4–6.5 eV). For the visible region, a tungsten lamp is used as a light source, and for UV region, there is a deuterium lamp. The initial light beam from the grating monochromator is split into two: one beam passes through a sample, and the other is used as a reference. Both beams are registered with a photomultiplier in the visible and UV region or with a PbS photoconducting cell in the IR region. Typical measurement settings were: Band Width 1.0 nm, Response medium, Data Pitch 1.0 nm, Scan Speed 100 nm/s. As the measure of absorbance, optical density (OD) was chosen. It is possible to measure absorbances up to $OD = 4$. However, above $OD = 3$ the instrument's response is nonlinear.

3. THE MECHANISMS OF DEFECT CREATION

The mechanisms that lead to the creation of lattice defects and their associates under irradiation are the same for large groups of solid-state materials.

The most universal is the fast ($\sim 10^{-15}$ s) so-called ‘knock-out’ mechanism, when an atom or ion in the lattice site is displaced after an elastic collision with an energetic particle (electron, proton, neutron, other ion), creating a vacancy and an interstitial. The energy transferred by such an incident particle to a particle in the lattice site has to be sufficiently high to separate the vacancy and interstitial, preventing the opposite process of recombination with the restoration of a regular structure. In the case of MgO, the threshold energy for displacing an Mg or O ion is about 60 eV (according to the energies measured in [15]). In the purest form, this mechanism is realized in the case of neutron irradiation.

The second mechanism is the slow ($\sim 10^{-10}$ s) adiabatic non-impact mechanism, in which electronic excitation (a self-trapped exciton (STE), a self-trapped hole recombining with conduction electron) is localized at regular lattice sites or as-grown defects, creating an unstable local configuration, which may relax through displacing an ion into a neighboring site. Since the process is slow, it requires less energy per lattice ion, typically, a few times less than the energy required to displace the same ion via elastic collision.

Unlike the knock-out mechanism, which is limited only by the energetic requirement, the non-impact mechanism has several criteria that have to be met in order for the process to be effective. For alkali halides these requirements have been discussed in [2–4, 16].

- 1) The energy of EE has to be higher than the threshold energy for the formation of a FD pair.
- 2) The time of localization of EE on the particular lattice site has to be sufficient for the displacement of ions to take place.
- 3) A dissociating configuration has to be oriented along tightly packed ionic rows to facilitate the removal of an interstitial from the respective vacancy via the crowdion displacement. In the case of fcc alkali halides, it is the $\langle 110 \rangle$ direction along halide rows.

The third mechanism of radiation damage is a new type of intrinsic localized mode with a large amplitude and frequency above the top of the acoustic phonon spectrum, which, according to theoretical predictions, may exist under the dense excitation of a crystal lattice predisposed to anharmonic interactions and cause a local phase transition (spreads over a large ion cluster) [7–9, 17]. These unusual excitations, also referred to as discrete breathers or discrete solitons, are expected to be especially strong in the WGMs built up of ions with very different masses – the frequency of discrete breathers can fall in a gap between acoustic and optical vibration branches. In pure MgO crystals with $E_{FD} > E_g$ and

close masses of anions and cations, such third mechanism is supposed to be ineffective, but may occur near impurity centers including heavier ions.

Lastly, large associates of defects are created by swift heavy ions [18–20]. Due to their charge and exceptionally large amounts of energy transferred to the host material per unit of path length, they interact with large areas of material, creating a ultra high density of electronic excitations and, therefore, cannot be described with elementary processes only (except for the areas distant from the track core). The structure and formation of a swift heavy ion track is still not clear. A model describing their formation is the ion explosion spike mechanism [21, 22]. Essentially, this model assumes that along their path SHI produce multicharged positive ions of the host material, and the resulting Coulomb force pushes them away from each other, creating an empty core surrounded by a stressed and chaotically distorted matter. The resulting state relaxes, to some extent, through ions draining lost electrons from outer regions and arranging themselves more uniformly, though still far from the original perfect lattice.

4. CRYSTAL STRUCTURE AND IMPERFECTIONS OF NaCl

4.1. A single crystal of NaCl

Sodium chloride is a colorless, odorless, relatively non-hygroscopic, and dielectric ionic crystal with a face-centered cubic lattice, which is made of Na^+ -ions ($r_c = 0.98 \text{ \AA}$) and Cl^- ions ($r_a = 1.81 \text{ \AA}$). The models of the three main crystallographic planes of NaCl lattice type are depicted in Fig. 1.

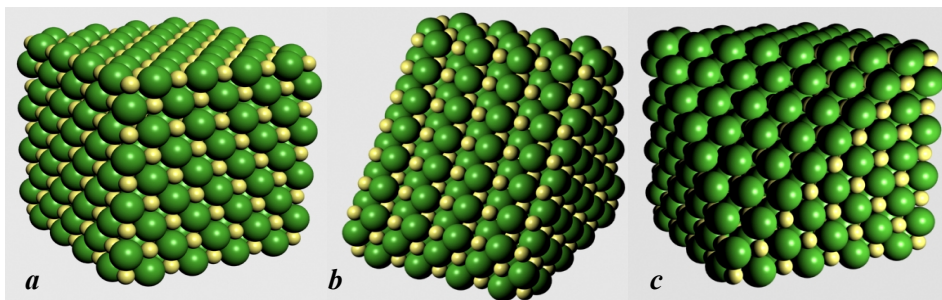


Figure 1. Crystallographic planes of NaCl: $a - (100)$, $b - (110)$, $c - (111)$

Some physical properties of this system are presented in Table. 1.

Table 1. Physical properties of NaCl.

Lattice type (25 °C, 100 kPa)	Face-centered cubic
Lattice constant (25 °C, 100 kPa)	5.640 Å
Coordination geometry	Octahedral (Na^+ , Cl^-)
Ionic radii (Goldschmidt), r_a/r_c	Na^+ : 0.98 Å, Cl^- : 1.81 Å, 1.85
Density (25 °C, 100 kPa)	2.165 g/cm ³
Molar mass	58.44 g/mol
Dielectric Constant ϵ_0	6.12 at 17–22°C
Melting point	801 °C / 1074 K
Debye temperature (20 °C)	322 K
Coefficient of Thermal Expansion:	$40 \times 10^{-6} \text{ 1/K}$ (at 0 °C)
Hardness (Mohs scale)	2.5
Thermal conductivity (8 K)	2.03 W/(cm·K)
Thermal conductivity (314 K)	0.069 W/(cm·K)
Refractive Index (589 nm):	1.5442
Band gap, E_g	8.7 eV

As a group, alkali halides exhibit a low resistance against ionizing radiation compared to MgO or Al₂O₃. However, within the group, susceptibility to radiation varies considerably: in some systems, where cation and anion radii are close so that there is enough space for ions to move (for example, KCl, RbCl), stable (with a lifetime of at least several seconds) anion Frenkel defects – F-H and α -I pairs – are efficiently created by e - h recombination and decay of excitons via a non-impact mechanism at all temperatures. In others, where $r_a > r_c$ (NaCl, KI, LiF), and anions are tightly packed, the efficiency of these processes at temperatures below 120 K is significantly lower compared to that at RT [2–4]. This means that, depending on the temperature, it is possible to achieve a high and low radiation resistance in the same system, which makes such systems especially interesting for radiation physics. NaCl has the additional advantage of having low hygroscopy, which makes it a convenient object for experiments compared to some other alkali halides, which have to be preserved in a dry atmosphere.

In NaCl at low temperatures, holes become self-trapped, creating the so-called V_K -centers [23], which decay at 150–180 K. Photons with the energy of 7.9–8.3 eV or 8.5 eV create excitons with $n = 1$ and $n = 2, 3$, respectively [24]. Like holes, excitons in NaCl also become self-trapped, when the hole component relaxes from an one-anion state into a two-anion state. Radiative recombination of self-trapped excitons with $n = 2$ and $n = 1$ gives rise to σ -emission 5.35 eV (lifetime 3.0×10^{-9} s) and π -emission 3.4 eV (lifetime 2.95×10^{-4} s). Exciton emission is quenched at RT and 100 K and only below 60 K becomes independent of temperature, with the luminescence yield close to 1 [26–27]. Transitions between different sublevels of excitons manifest in the absorption spectra as bands with maximums at 2.0, 2.02, and 2.25 eV ($1s \rightarrow 2p$) or 2.65 eV ($1s \rightarrow 3p$), with an electron being the absorbing component. The hole component of an exciton absorbs at 3.61 eV [24].

4.2. Intrinsic and impurity defects in NaCl

The most basic intrinsic defects in the anion sublattice of NaCl are anion vacancies (v_a , α -centers) and interstitial Cl⁻ ions (I-centers). Having an effective electric charge, these centers are able to capture electrons or holes, producing effectively neutral F-centers ($v_a e$) and H-centers (Cl₁⁰, or (Cl₂)_a⁰), respectively. In many alkali halides (KCl, KBr, RbCl, RbBr), an H-center is oriented along $\langle 110 \rangle$ (anion rows) [28], but in NaCl it is oriented along $\langle 111 \rangle$ [24]. At a certain distance between centers, a direct conversion of an α ,I-pair into an F-H pair (or backwards) by relocation of an electron may take place. An F-center may also capture an additional electron, becoming an F'-center, the absorption of which strongly overlaps with F-center absorption. Cation counterparts include cation vacancies, Na⁺-interstitials and holes captured at cation

vacancies – V_F -centers ($v_c h$). Here and hereafter superscripts in structural formulae indicate the effective charges in relation to the neutral lattice.

These basic defects may aggregate into more complex centers: F_2 ($v_a e v_a e$), F_2^+ ($v_a e v_a$), bivacancies ($v_a v_c$), H_2 , X_3^- (trihalide molecules (Cl_3^-)_{aca} along $\langle 100 \rangle$), and other.

The main impurities, which usually exist even in highly pure NaCl crystals, are Li^+ , K^+ , Ca^{2+} , Br^- , and I^- ions. The Ca^{2+} concentration is especially high (~20 ppm) in artificial crystals, because the distribution coefficient of Ca^{2+} between a solid and melt is close to 1, so it is hard to lower the concentration of this impurity with zone melting. The absorption and emission bands of the defects and excitons situated near these ions have shifted maximums compared to the respective centers in regular lattice sites. For example, the excitons near Br^- have emission shifted from 3.4 to 3.8 eV, near-Li excitons emit at 3.38 eV, and $H_A(Li)$ centers absorb at 3.35 or 4.6 eV, compared to the “pure” H-absorption of 3.85 eV. Their location near impurities may also improve thermal stability of defects: H-centers become mobile at 30–42 K, but $H_A(Li)$ centers are immobile up to 130–150 K [24]. Many defects in NaCl have identified absorption and emission bands. The absorption maximums of some of these centers are presented in Table 2 [24, 29].

Table 2. Absorption maximums of some defects in NaCl.

Center	Structure	Absorption maximum		Additional details
		[eV]	[nm]	
α	v_a	7.16	173	Abs. of Cl^- ions around v_a , emission 2.95 eV @ 80 K
V_K	$(Cl_2)_{aa}^+$	3.28	378	
H	$(Cl_2)_a^0$	3.85	322	
X_3^-	(Cl_3^-)	4.9, 5.35	235, 232	Centers with different configuration
F	$v_a e$	2.746	458	@ 4.2 K, half-width 0.27 eV
F'	$v_a e e$	2.0	620	Overlaps with F Abs. band
F_2	$v_a e v_a e$	1.708	725	
F_2^+	$v_a e v_a$	1.203	1030	
R_1		2.27	545	F_3 -centers with different configuration
R_2		2.078	596	
N_1		1.5	826	F_4 -centers with different configuration
N_2		1.439	861	
$H_A(Li)$	$Li^+(Cl_2)_a^0$	3.35, 4.6	370, 270	

5. RESULTS OF EXPERIMENTS WITH NaCl

5.1. Non-impact defect creation at cryotemperatures

It was already mentioned, that in NaCl at liquid helium temperatures the efficiency of non-impact creation of long-lived Frenkel defects is about an order of the magnitude lower than at 300 K, unlike in KCl and similar systems, where the efficiency of this process does not show significant dependence on temperature.

If we look at the necessary requirements for non-impact mechanism (Chpt. 3) in NaCl, then we will see that the second and the third ones are not met. Firstly, the vibration frequency of a decaying exciton overlaps with the region of lattice vibrations, so this excitation quickly relaxes into a package of phonons. Secondly, in NaCl the excited configuration is aligned along $\langle 111 \rangle$, so the double-Cl configuration (a precursor to an H-center) interacts not with the nearest Cl anions, but with the nearest Na cations, therefore hampering the crowdion mechanism of interstitial displacement. This is strongly facilitated by the fact that a decrease in the temperature causes contraction of the crystalline lattice, making it more compact and hampering the rotation of H-centers and migration of ions. And, essentially, this means an increase in the E_{FD} over the E_g . This is why the efficiency of FD creation via the decay of EE at low temperatures is low: the probability of decay into a pair of defects (instead of radiative decay or relaxation via a packet of phonons) is low by itself, and even if it realizes, H centers cannot migrate far enough from their counterpart F centers, and such pairs recombine back into regular lattice. This is probably also the reason why it is very difficult to register the creation of α -I pairs at low temperatures: the region of spontaneous recombination for charged defects is even larger than for neutral F-H. In comparison, for KCl all the three criteria are met at all temperatures.

Due to the low FD creation efficiency at low temperatures, sensitive TSL and PSL methods are preferred over direct optical absorption methods. Fig. 2 presents the TSL curves of NaCl (Leitz) for integral signal (1.8–6 eV) and for the 3.4 eV emission of triplet STE, which arises at the tunnel recombination of an F-center electron with a self-trapped hole (V_K) [I]. It had been established ([24] and references therein) that the TSL peak at 14 K arises at the recombination of a mobile anion interstitial with an F-center, while the remaining conduction electron recombines with a V_K -center. The less intensive peak at 21 K has the same origin; no peaks are registered at 22–32 K. In NaCl, interdefect distances in F-H pairs are short, so anion interstitials need the minimal number of hops before recombining with F-centers. According to Fig. 2, a significant part of the 3.4 eV TSL light sum is concentrated in the peak at 35.5 K. It has been shown earlier by our group and other groups that in this temperature region the annealing of H-center EPR signal takes place. However, this peak arises not due to the recombination of mobile H-centers with

F'-centers and consequent recombination of the remaining electrons with V_K -centers, as was assumed before. Under our experimental conditions, F'-centers practically did not accumulate due to destruction by the red (heat) emission of the cathode. The latest experiments showed that NaCl is a unique system, in which the energy of a close F-H pair exceeds the level of a relaxed triplet exciton. At 35 K, after one or two hops, an H-center recombines with its related F-center counterpart, and this recombination goes through the triplet state of anion exciton. It should be noted that the TSL emission of 3.4 eV resides on the practically temperature-independent tunnel pedestal, which disappears only after thermal annealing of V_K -centers at 170–180 K. A V_K -center is one of the tunnel pair components. The other component could, possibly, be an electron localized at a bivacancy, the number of which can be increased by a rapid cooling down from 400 to 10 K.

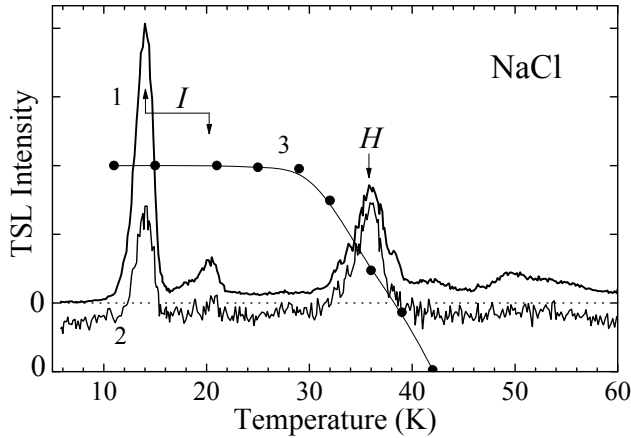
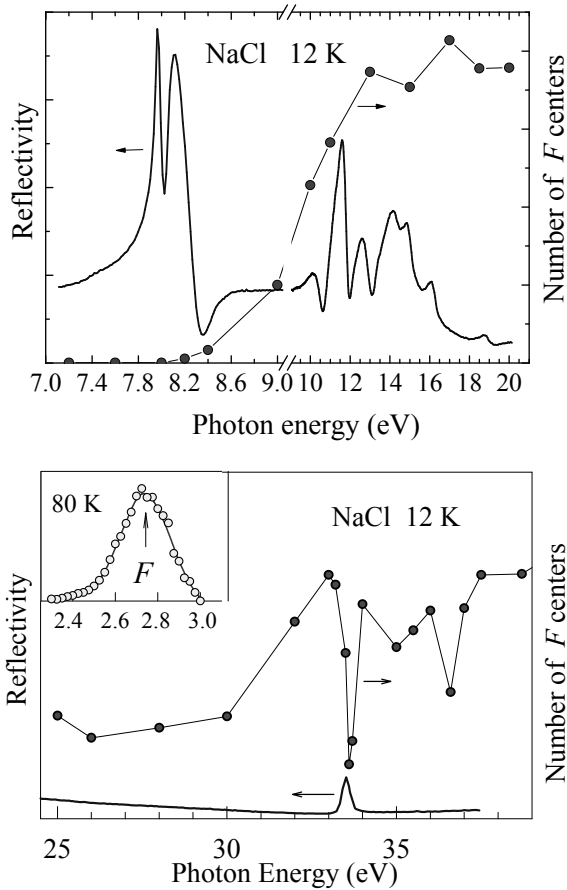


Figure 2. TSL for emission 3.4 eV (1) and integral signal (2, channel sensitivity is lower) in NaCl (Leitz) irradiated with 8 keV electrons at 5.8 K. $\beta = 10$ K/min. (3) – impulse annealing of H-centers EPR signal in X-irradiated NaCl [24].

To study the individual efficiency of the low-temperature non-impact creation of long-lived defects by excitons or $e-h$ pairs, we have measured the creation spectra of F-centers by VUV radiation at 12 K (the first such spectrum at 300 K was measured in 1964 [30]). The resulting spectra of F-center creation are presented in Fig. 3 and 4 [II].

Our experiment was performed at an undulator beamline in MAX-Lab. The highly pure single crystal of NaCl was irradiated perpendicular to (100) plane by a prescribed number of photons at each of several energies. For an equal quantum irradiation dose, sodium salicylate was used as a reference. After irradiation, a pause of 30 s was made to eliminate short-lived F-H pairs. Then, the irradiated crystal was stimulated by 2.7 eV photons (maximum of F-center

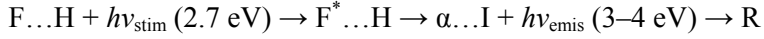
absorption), resulting in rapidly damping PSL (stimulation spectrum of this PSL coincides with the F-center absorption band – see inset on Fig. 4). This luminescence was selected through a group of optical filters (3–5 eV), and its light sum measured with a photon-counting head was taken as a measure of the F-H pairs formed under irradiation with SR.



Figures 3 and 4. The reflection spectra and creation spectra of F-H pairs measured at 12 K for a highly pure NaCl single crystal. The inset shows the stimulation spectrum of PSL at 80 K.

This low-temperature method was elaborated at the Institute of Physics (Tartu) [31]. Photons of 2.7 eV excite (not ionize!) the electron component of an F-center in NaCl, increasing the effective radius of the center and facilitating tunnel relocation of an electron from an F^* center to a nearby H center accompanied by the emission of 3–4 eV (depending on intercomponent distance). Such radiative recharge of F and H centers transforms them into an

α -I pair, effectively charged components of which attract to each other and recombine non-radiatively, restoring the regular crystalline structure (R). The whole process may be presented as follows:



According to these results, the exciting photons in the region of exciton absorption (7.8–8.4 eV) do not cause the creation of F centers. A weak PSL (possibly, impurity-related) is detected in the spectral region slightly above the band gap ($E_g = 8.9 \text{ eV}$), where s -conduction electrons are formed. However, a sharp rise of the PSL light sum takes place, when the exciting photons of $h\nu = 12\text{--}16 \text{ eV}$ form hot d -conduction electrons, but do not cause the formation of secondary anion excitons (i. e. the multiplication process has not started yet [32, 33]). Therefore, the energy released at the recombination between d -conduction electrons and p -valence holes is sufficient for the creation of stable F-H pairs with a relatively large interdefect separation.

The number of F-H pairs (i.e. the PSL light sum) changes only slightly with the rise of the exciting photon energy from 12.5 to 27 eV (see Figs. 3 and 4), while the creation efficiency of FD doubles at 28–33 eV (Fig. 4). According to our previous data on the multiplication of electronic excitations in a number of alkali halides, such photons can form up to three electron-hole pairs in NaCl [32]. However, only two hot e - h pairs contribute to the creation of stable F-H pairs.

Of particular interest is the creation of F centers by 33–34 eV photons that form cation excitons. It was shown earlier [32] that a cation exciton ($\sim 33.4 \text{ eV}$) decays into an anion exciton and several e - h pairs. The energy excess of about 24 eV remaining after the formation of an anion exciton is enough to form two e - h pairs, but only one of them will be sufficiently hot for the creation of a pair of FD. A deep dip of the creation efficiency of F-H pairs is observed in the region of cation exciton absorption. This dip remains even if the reflection losses (narrow reflection peak at 33.4 eV – see Fig. 4) are taken into account. So, only a hot e - h pair, formed together with an anion exciton and a cold e - h pair at the decay of a cation exciton, is able to create an F-H pair at 12 K. Consequently, the recombination of a hot conduction electron with a hole causes the creation of a pair of anion FD in a NaCl crystal with $E_{\text{FD}} > E_g$ at cryotemperatures.

Having these results, we have conducted additional experiments to study the difference between the defect creation efficiency by cold and hot e - h pairs at room temperature. For this, we used KrF ($h\nu = 4.99 \text{ eV}$, laser power = 5 mJ, impulse duration = 5 ns, laser frequency = 20 Hz) and ArF ($h\nu = 6.42 \text{ eV}$, 5 mJ, 10 ns, 20 Hz) excimer lasers in the two-photon absorption mode. In this mode, exciting photons are absorbed not by one, but in pairs, which effectively doubles the excitation energy (9.98 eV for KrF and 12.84 eV for ArF) without the disadvantage of high absorption coefficients typical for photons with their

energy above E_g . This way, the excitation in the whole bulk of object was obtained, so the role of surface defects could be neglected.

Excitation by 10 eV selectively produces cold $e-h$ pairs, and by 12.84 eV – hot ones. Highly pure single crystals of natural NaCl and NaCl (Leitz) were irradiated along $\langle 100 \rangle$ by one of the lasers for 15–30 min (to achieve a certain dose), and then their absorption spectrum along the laser spot was measured. The results of these measurements are presented in Fig. 5 (the spectra are not normalized to the sample thickness and the doses of laser irradiation).

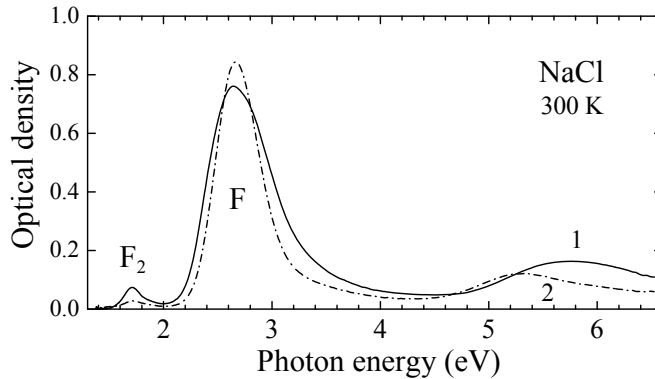


Figure 5. Spectrum of optical absorption in natural NaCl (1) and NaCl (Leitz) (2) induced by the emission of (2) KrF ($5 \times 2 = 10$ eV) or (1) ArF ($6.42 \times 2 = 12.84$ eV, natural NaCl) excimer laser at 300 K.

In both cases, not only F and H, but also more complex F_2 and trihalides Cl_3^- are effectively created. However, there is a notable difference between these two cases in the number of F_2 -centers (relatively higher in the case of hot $e-h$ pairs) and in the absorption region of Cl_3^- centers (4.5–6.5 eV), which is partially caused by the quenching effect of single-photon absorption and partially by the different defect creation efficiency. This result illustrates the fact that the difference in the defect creation efficiency by cold or hot electron-hole pairs in NaCl still remains even at RT, when $E_{FD} < E_g$.

The importance of defect creation by hot $e-h$ pairs at RT was also revealed in a similar experiment on KCl: the comparison of the absorption spectra was made between single crystals irradiated by X-rays or ArF-laser, whereas one of the laser-irradiated crystals underwent a preliminary plastic deformation along (100). The results are depicted in Fig. 6 [VIII].

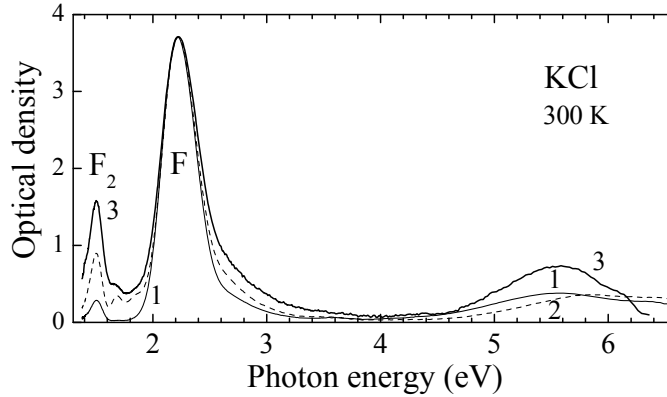


Figure 6. Optical absorption spectra of KCl single crystals irradiated with X-rays (1), irradiated with ArF laser for non-deformed (2) and deformed (3) samples at 300 K.

Unlike laser, creation of defects with X-rays is a complex multiple-stage process, at the end of which secondary $e-h$ pairs and secondary excitons are created, whereas the number of $e-h$ pairs is several times larger than the number of excitons. However, the experiment has clearly shown that creation of F- and F_2 -centers is more efficient in the case of an ArF-laser, providing the “pure” $e-h$ process: for the X-irradiated crystal, the ratio between intensities of the F and F_2 absorption bands was 17.5, and for the ArF-irradiated crystal it was 4.1. Plastic deformation increased the relative number of F_2 -centers in the ArF-irradiated crystal even further, so the ratio of 2.3 was achieved.

We assume that the excitons produced by X-rays do not create F_2 -centers and even cause the destruction of defects created via the $e-h$ mechanism. The inefficiency of F_2 -centers creation by excitons has been shown for LiF [34]. In that work, the process of transforming F-centers into F_2 -centers has also been suggested. Recombination of electrons and holes leads to the creation of F-H pairs. Some of F-centers are ionized by holes, becoming anion vacancies, which are mobile at room temperature. These vacancies migrate to other F-centers, producing F_2^+ -centers, which, after capturing an electron, become neutral F_2 -centers.

5.2 The Franck-Hertz effect as luminescent protection of NaCl:TI⁺

The solid-state analogue of the Franck-Hertz effect (SSAFHE) is the process of resonant excitation of luminescent impurity centers and structural defects by hot (non-relaxed) conduction electrons and/or valence holes in wide-gap materials (see [36] and references therein). As charge carriers lose their initial energy in this process, it is, obviously, one of the ways to reduce the probability of hot

$e-h$ recombinations, the energy of which might exceed E_{FD} and satisfy the energetic criteria for non-impact defect creation. SSAFHE is also of obvious interest for fundamental studies and various technical applications, such as the elaboration of novel spectral transformers for neon luminescent tubes and xenon plasma display panels. The main difficulty with studying the direct excitation by conduction electrons or valence holes is that this fast process is hardly distinguishable from the low-inertial excitonic mechanism.

Fig. 7 shows a simplified energy-band diagram of a NaCl single crystal doped with mercury-like Tl^+ ions with the $6s^2$ ground-state configuration [II]. The minimum energy for the direct optical formation of an anion exciton with $n = 1$ equals $E_c = 8$ eV, the energy gap is $E_g = 8.75$ eV, and the total width of the valence band (v-band) is $E_v \approx 3$ eV. Fig. 7 also demonstrates the energy levels of a Tl^+ impurity center in NaCl: Tl^+ , which are located within the energy gap and correspond to the 1S_0 , 3P_1 , and 1P_1 states of a free Tl^+ ion. The position of the 1P_1 level (~ 6.2 eV) with respect to the bottom of the conduction band (c-band) was experimentally determined by measuring the excitation spectra of recombination luminescence and photoconductivity.

Fig. 8 demonstrates the excitation spectra of A emission (4.27 eV, $^3P_1 \rightarrow ^1S_0$) of Tl^+ centers in NaCl: Tl^+ measured using synchrotron radiation at 8 K [II]. The spectra were measured for time-integrated luminescence as well as for the emission detected within two time windows (length Δt) correlated with the excitation pulses of synchrotron radiations (delayed by δt). The parameters for the fast emission component were $\Delta t = 10$ ns and $\delta t = 2$ ns and for the slow one – $\Delta t = 250$ ns and $\delta t = 200$ ns. The spectra contain three bands: the A excitation (absorption) band peaked at 4.78 eV corresponds to $^1S_0 \rightarrow ^3P_1$ electron transitions in a free Tl^+ ion; the C band (6.2 eV) is related to $^1S_0 \rightarrow ^1P_1$ singlet–singlet transitions, and the so-called D-band (a non-elementary band at ~ 7.7 eV directly adjoins the exciton absorption bands), which is caused by the excitation and ionization of the chlorine ions surrounding an impurity ion.

According to Fig. 7, a photon of $h\nu > 20$ eV forms a hot conduction electron, which is able to create a secondary $e-h$ pair due to the non-radiative Auger transition (case *a*, arrow lines 2 and 2'), while the energy excess of a hot conduction electron (with respect to the bottom of the c-band), formed by an exciting photon of $h\nu = 18-20$ eV is sufficient to create a secondary exciton (case *b*, 3 and 3'). An even lower energy of exciting photons ($h\nu = 15-17$ eV) is needed for the direct excitation of impurity centers by hot conduction electrons, i.e., for the realization of a solid-state analogue of SSAFHE in NaCl: Tl^+ (case *c*, arrow lines 4 and 4' or cased, 5 and 5').

A comparison of the excitation spectra of impurity center luminescence in doped crystals with the photoemission spectra from thin films helped to separate SSAFHE from other mechanisms of photon multiplication in WGM. Earlier, this comparison had been made for RbCl: Tl^+ and RbCl: Ag^+ crystals [35, 36].

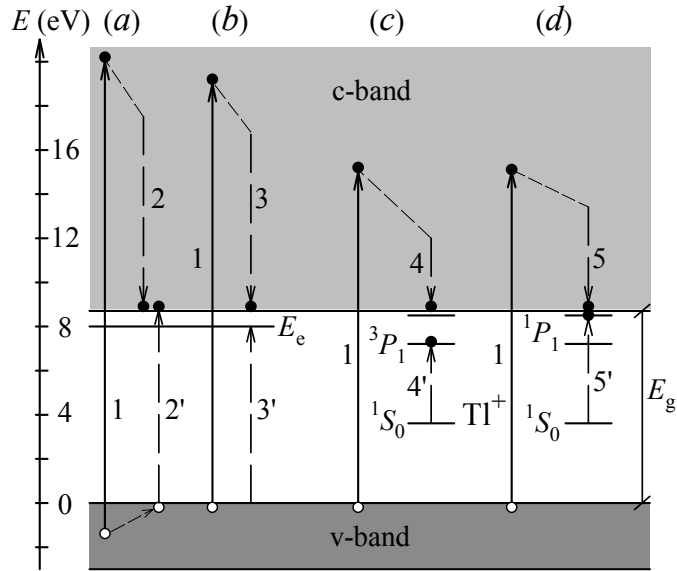


Figure 7. A simplified energy-band diagram for a NaCl:TI⁺ crystal. The multiplication processes connected with the creation of a secondary $e-h$ pair (case *a*) or a secondary anion exciton (case *b*) by a hot conduction electron as well as the excitation of a TI⁺ impurity center by a hot electron (cases *c* and *d*) due to non-radiative Auger transitions ($2 \rightarrow 2'$, $3 \rightarrow 3'$, $4 \rightarrow 4'$, $5 \rightarrow 5'$). All the processes start with the absorption of an exciting photon (arrow line 1). The inclined dashed arrow lines demonstrate non-radiative transitions at carrier relaxation inside energy bands.

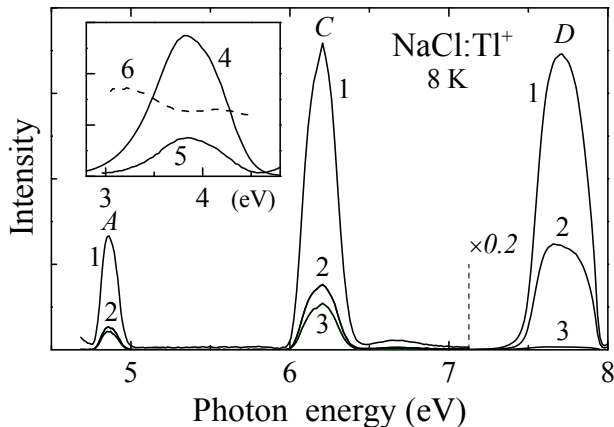


Figure 8. The excitation spectra of A emission (4.27 eV, $^3P_1 \rightarrow ^1S_0$) of TI⁺ centers measured for time-integrated (curve 1), slow ($\Delta t = 250$ ns and $\delta t = 200$ ns, curve 2) and fast ($\Delta t = 10$ ns and $\delta t = 2$ ns, curve 3) components in NaCl:TI⁺ at 8 K. Inset shows the emission spectra measured for slow (4) and fast (5) components and the intensity ratio spectrum for slow/fast emissions (6) in NaCl on the excitation by 7.7 eV photons at 8 K.

According to photoelectron spectra of an extra pure NaCl evaporated film measured at 295 K (see [II] for details), photons of $h\nu = 15.7$ eV already create electrons with $E_{\text{kin}} = 4.3$ eV, which are able ($\chi = 0.7$ eV should be taken into account) to excite TI^+ up to the $^3\text{P}_1$ state. A further radiative transition to the ground state ($^3\text{P}_1 \rightarrow ^1\text{S}_0$) results in the A emission of TI^+ centers. In case $h\nu = 16.6$ eV, hot conduction electrons excite TI^+ centers even up to a higher $^1\text{P}_1$ singlet state. The inset on Fig. 8 shows the emission spectra measured for the fast ($\Delta t = 10$ ns, $\delta t = 2$ ns) and slow ($\Delta t = 250$ ns, $\delta t = 200$ ns) component in NaCl at the excitation by 7.7 eV photons at 8 K. Such exciting photons fall within a non-elementary D excitation band of TI^+ centers adjacent to the exciton absorption. The intensity ratio spectrum for the slow and fast emission components makes it possible to separate the A emission of TI^+ centers (~ 4.2 eV) and a more inertial emission (~ 3.35 eV) associated with self-trapped excitons.

By way of concluding this section, it should be mentioned that Fig. 7 presents a significantly simplified energy diagram of a NaCl crystal with a relatively narrow valence band ($E_v \approx 3$ eV). The separation of SSAFHE from the fast excitonic and $e-h$ mechanisms of photon multiplication in binary and complex metal oxides runs into obvious problems due to a sharp rise of E_v up to the value of E_g in these WGM. For instance, the value of $E_v \approx 6.6$ eV can be experimentally estimated from the spectra of fast intraband luminescence measured under excitation of MgO crystals by nanosecond single 300 eV electron pulses [37].

6. CRYSTAL STRUCTURE AND IMPERFECTIONS OF MgO

6.1. A single crystal of MgO

Like NaCl, magnesium oxide is a colorless, odorless, non-hygroscopic, and dielectric ionic crystal with the fcc lattice type, although the bonds between ions are not purely ionic, but also partially covalent. The crystal consists of double-charged Mg^{2+} -ions ($r_c = 0.74 \text{ \AA}$) and O^{2-} ions ($r_a = 1.36 \text{ \AA}$), and their ratio of ~ 1.84 is practically the same, as in NaCl. As the crystalline structures are the same in both crystals, Fig. 1 can be used to visualize the main crystallographic planes in MgO. Some general physical properties of magnesium oxide are presented in Table 3.

Table 3. Physical properties of MgO.

Lattice type (25 °C, 100 kPa)	Face-centered cubic
Lattice constant (25 °C, 100 kPa)	4.212 Å
Coordination geometry	Octahedral (Mg^{2+} , O^{2-})
Ionic radii (Goldschmidt), r_a/r_c	Mg^{2+} : 0.74 Å, O^{2-} : 1.36 Å, 1.84
Density (25 °C, 100 kPa)	3.58 g/cm ³
Molar mass	40.3044 g/mol
Dielectric Constant ϵ_0	9.8
Melting point	2852 °C / 3125 K
Debye temperature	743 ± 8 K
Coefficient of Thermal Expansion:	$8.0 \times 10^{-6} \text{ 1/K}$ (at 100 °C)
Hardness (Mohs scale)	5.8
Thermal conductivity	45–60 W/(cm·K)
Refractive Index (589 nm):	1.7366
Band gap, E_g	$\sim 7.8 \text{ eV}$

The charge distribution symmetry between ions and a large band gap in MgO make it similar to alkali halides and other dielectrics. However, a wide valence band and high dielectric constant are more natural to semiconductors. Nowadays, the exact value of the valence band width in MgO is still unknown, but different calculations and empirical estimations suggest that it is at least 6 eV wide. This means, that, unlike in dielectrics with a narrow valence band, in MgO, holes are able to occupy different energetic levels within the band, so the position of an electron after excitation into the conduction band by a photon cannot be obtained simply by adding photon energy to the top of valence band. This also means, that secondary excitons and electron-hole pairs are not created

by photons with energy $\sim 2E_g$, since this energy will be split between both the primary electron and hole. Multiplication of electronic excitations begins to take place only at higher exciting photon energies. In MgO, this process begins at 19–25 eV [38, 39]. Thermal quenching of excitons occurs at 80 K, and at higher temperatures all excitons undergo ionization.

One of the most notable properties of MgO is that neither electrons or holes, nor excitons become self-trapped in regular lattice sites at any temperature [71, 72]. At first, there were arguments about the existence of STE, as the low-temperature emission of 6.9 eV was assumed to arise from their radiative decay [40], although theoretical calculations supported the absence of self-trapping. Later experiments confirmed that 6.9 eV emission is related to impurity centers: it was absent in very pure crystals and enhanced in Ca-doped crystals, therefore, it could not be ascribed to the luminescence of self-trapped excitons. In contrast to alkali halides, the lowest energy state of excitons in MgO is a singlet state with $j = 1/2$, while a triplet state with $j = 3/2$ possesses a higher energy. Such an energy structure of excitons fits naturally into the scheme that at low temperatures excitons and holes do not undergo transition into a self-trapped state in regular lattice regions. This property is very important, as it makes it impossible to meet the localization requirement for non-impact FD creation. Combining it with the fact that in MgO $E_{FD} > E_g$ it is clear, why this system is one of the most radiation-resistant.

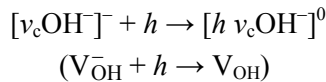
However, real crystals are never ideal systems, as they always have as-grown structural and impurity defects, which may provide suitable conditions for the realization of the non-impact mechanism of FD creation. It was also theoretically shown, that holes and excitons might become self-trapped at outer and inner surfaces of a crystal [41]. Once there is a localized EE, the situation is similar to NaCl at low temperature, where $E_{FD} > E_g$, but holes are localized, and so defects are created in recombinations of these holes with hot electrons, which are produced in large numbers during irradiation with swift heavy ions. This is why we turned our attention mainly to the possibilities of the same process in MgO, which, in turn, means that our primary object of interest were holes localized at various lattice irregularities and ways of decreasing the number of hot electrons (for example, by the transfer of their energy to luminescent centers). The exact value of the energy needed for the formation of an FD pair in anion sublattice of MgO is unknown, but it can be roughly estimated. Knowing that the energy required for the slow adiabatic non-impact mechanism is up to two times lower than for the impact mechanism, which in MgO requires about 60 eV per particle (calculation based on [15]), it is possible to estimate the non-impact E_{FD} for anion FD as ~ 30 eV. This energy lies in the region of multiplication of electronic excitations, so there is a strong competition with the Auger process, and the overall efficiency of defect formation channel is low under low densities of electronic excitations.

6.2. Intrinsic and impurity defects in MgO

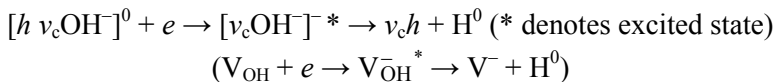
Due to the double charge of ions in MgO, the basic Frenkel defects – vacancies and interstitials – have also a double effective charge, which makes them deeper traps for holes and electrons compared to NaCl. Besides neutral F ($v_a ee$) and V ($v_c hh$, or $O^- v_c O^-$ – in this case absolute charges are given) centers, there are also charged F^+ ($v_a e$) and V^- ($v_c h$, or $v_c O^-$) centers. Single anion vacancy has not been found in MgO yet.

Besides isovalent impurities (Ca^{2+} , Be^{2+}), MgO crystals usually contain trivalent Al^{3+} and 3d-metal ions (Cr^{+3} , Fe^{3+}), the excessive charge of which is compensated for by cation vacancies or monovalent alkali metal ions. These vacancies give rise to the whole group of V-type hole centers (holes are captured by neighboring oxygen ions) depending on their effective charge and proximity of impurities. These hole centers are denoted with capital V, and if a hole center containing a cation vacancy also contains an impurity ion, the latter is indicated by a subscript, e.g., V_{Al} center. If the center has no effective charge with respect to the neutral lattice, the superscript can be omitted: V, V^- , V_{Al} , V_{OH} , V_F . For MgO, this notation has been widely accepted since the work by Henderson [42]. The notation is outdated, and contemporary authors sometimes use different notations. However, currently, there is no commonly accepted new notation, which is why the old notation is used in this work. V-centers are the main type of intrinsic defects in unirradiated crystals. All of them are paramagnetic and have optical absorption bands related to the relocation of a hole between equivalent O^{2-} positions around vacancy [43].

The most troublesome are V_{OH} centers [$h v_c OH^-$]⁰, which are formed under irradiation, when as-grown V_{OH}^- -centers caused by the presence of humidity in the starting material capture holes (h):

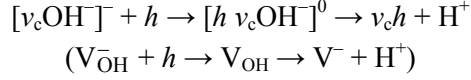


In the process of recombination with conduction electrons (e) forming under irradiation, the OH-group dissociates into O^- and H^0 , and with separation of the hydrogen V_{OH} center is converted into a V^- center.



H^0 are highly mobile due to their small size, and they are prone to combining into H_2 molecules and gathering into gas bubbles, which cause the cloudiness of crystals [29].

In [5] another mechanism of conversion of a V_{OH}^- center into a V^- was proposed:



Protons, forming in this reaction, migrate away and localize mainly as $Mg(OH)_2$. However, the probability of this mechanism is questionable. Firstly, the energy released at the hole capture (~ 0.84 eV [5]) is significantly lower than the bond energy of OH^- in V_{OH}^- (~ 4.8 eV [44]), whereas the energy released at recombination with an electron is sufficient to break the O-H bond. Secondly, according to measurements, the creation efficiency of V-centers increases with temperature, but rapidly drops down to zero at $T \geq 335$ K, i.e., above the temperature of thermal dissociation of V_{OH} .

The presence of monovalent Li^+ and Na^+ ions (effective negative charge – hole trap) is also possible, leading to the formation of $[Li]^0$ (hLi^+) and $[Na]^0$ (hNa^+) hole centers.

Heating of a γ -irradiated crystal to the temperature of v_c mobility leads to the appearance of $v_c v_a e$ -centers (bivacancy with trapped electron, the so-called P-centers [45]). After irradiation with fast neutrons, a linear trivacancy with two trapped electrons ($v_a e v_c v_a e$) was observed. Intense irradiation or heating of an irradiated crystal leads to the formation of pairs and more complex associations of the aforementioned defects. The optical properties of some of the defect centers are presented in Table 4 [46–60].

There is little data on interstitials in MgO. The most direct experimental proof of anion interstitials was presented in [61], where the EPR signal of the molecular O^{2-} ion near a cation vacancy was observed in neutron-irradiated crystals after heating to 550 K. According to theoretical calculations [62–64], an oxygen interstitial in MgO is a neutral defect, which is stabilized in a dumbbell form $O^- - O^-$ oriented along $\langle 110 \rangle$.

Table 4. Optical properties of some defects in MgO

Center	Structure	Absorption [eV]	Emission [eV]	Additional details
F ⁺	$v_a ee$	4.92	3.13	Abs. FWHM ~0.62 eV (RT)
F	$v_a e$	5.01	2.4	Abs. FWHM ~0.77 eV (RT)
F ₂	$v_a ee v_a ee$	3.53 1.27	3.25 1.1	
F ₂ ⁺	$v_a ee v_a e$		2.61	
F ₂ ²⁺	$v_a e v_a e$	3.85	2.81	
V ⁻	$v_c h$ ($v_c O^-$)	2.33		Abs. FWHM ~0.97 eV (77 K)
V ⁰	$v_c h h$ ($O^- v_c O^-$)	2.37		Abs. FWHM ~0.95 eV (77 K)
V _{Al}	$Al^{3+} O^{2-} v_c h$	2.33		Abs. FWHM ~0.97 eV (77 K)
V _{OH}	$h v_c OH^-$	2.33 or 2.19		Abs. FWHM ~0.88 eV (77 K)
[Li] ⁰	$h Li^+$	1.83		
[Na] ⁰	$h Na^+$	1.58		
Cr ³⁺		2.02 2.79 4.40 5.85	1.78, 1.77, 1.76, 1.74, 1.72, 1.67, 1.66 1.6–1.4 2.3, 3.44	Series of cubic and tetragonal centers' emission lines with phonon sidebands Emission bands related to rhombic centers Charge transfer
Fe ²⁺		1.48, 1.24		⁵ T _{2g} (D) → ⁵ E _g (D)
Fe ³⁺		5.71, 4.43	3.2	Charge transfer
Mn ²⁺			2.03, 1.68	
Mn ⁴⁺			1.88, 1.85	Cubic and tetragonal centers
Sn ²⁺		5.6	3.0	
			5.0	Si – related emission
			5.2	F, Cl – related emission
Al ³⁺			5.3	Near-Al recombinations
			5.8	Li-related emission
Be ²⁺			6.2	Near-Be recombinations
Ca ²⁺			6.9	Near-Ca recombinations
OH ⁻		6.4		

6.3. Thermostimulated luminescence in MgO

TSL of pure and doped MgO crystals is well-studied in the range of 77–500 K. Less is known about the peaks below 77 K and above 500 K. In unirradiated MgO there are three emissions, for which TSL can be registered: red (~1.7 eV) emission of Cr ions related to the release of holes and dominating in the peaks above 400 K, UV (5.2–5.7 eV) emission caused by recombination of electrons with the holes localized near cation vacancies or impurities, and emission ~2.9 eV related to the centers produced by deformation and cleaving of crystals; the emission arises at both electron and hole recombination stages. An interpretation of these last centers and related emission will be provided in the Results section. The thermal characteristics of most confidently identified defect centers in MgO are presented in Table 5 [65].

Table 5. Processes related to some identified TSL peaks in MgO, $\beta = 10$ K/min.

Peak position, K	Related process	Brief notation
185	$h\text{Na}^+ \rightarrow \text{Na}^+ + h$	$[\text{Na}]^0 \rightarrow [\text{Na}]^- + h$
190	$\text{Cr}^+ \rightarrow \text{Cr}^{2+} + e$	
230	$h\text{Li}^+ \rightarrow \text{Li}^+ + h$	$[\text{Li}]^0 \rightarrow [\text{Li}]^- + h$
335	$h v_c\text{OH}^- \rightarrow v_c\text{OH}^- + h$	$V_{\text{OH}} \rightarrow V_{\text{OH}}^- + h$
345	$v_c h h \rightarrow v_c h + h$	$V^0 \rightarrow V^- + h$
370	$\text{Al}^{3+}\text{O}^{2-} v_c h \rightarrow \text{Al}^{3+}\text{O}^{2-} v_c + h$	$V_{\text{Al}} \rightarrow V_{\text{Al}}^- + h$
420	$v_c h \rightarrow v_c + h$	$V^- \rightarrow v_c + h$

According to [66], all the TSL peaks at 370, 440, 484, and 545 K ($\beta = 2$ K/s) are related to the release of holes. The peaks at temperatures of 750 K and higher are probably related to the dissociation of defect complexes and migration of interstitials.

7. RESULTS OF EXPERIMENTS WITH MgO

7.1 Impurity ions as luminescent protection against creation of FD

The relatively small size of Mg^{2+} cations makes it difficult to introduce most luminescent ions into the MgO lattice. One of the few suitable choices is a Cr^{3+} ion, which usually exists in small concentrations even in highly pure MgO crystals and allows achieving concentrations of up to several hundreds of ppm.

To study the possibility of SSAFHE in MgO, we have used the excitation by an electron beam (5 keV, 50 nA/mm², the equipment is described in 2.2.2) and MgO single crystals doped with ~100 ppm of Cr^{3+} . Excitons are ionized at temperatures above 80 K, and at lower temperatures the creation efficiency of free excitons by 3–30 keV is at least an order of magnitude lower than of separated e and h . Therefore, mainly rapid e – h recombinations at impurity centers are in real competition with fast energy transfer from MgO matrix to defects via SSAFHE.

The CL spectrum of MgO:Cr crystal has been measured at the cooling down from 400 to 6 K at ~10 K/min (Fig. 9a) [II]. To avoid high irradiation dose, short-run ~30 s pulses with pauses of 60 s between the pulses were made down to 45 K. From 45 to 6 K, the cooling speed is rather fast, so in this region the irradiation was constant. The emission of Cr-ions (~1.76 eV) was selected through a double monochromator. Switch-off of the electron gun lead to a drop in luminescence intensity by 3–4 orders of magnitude during the first 1–2 s. Switch-on of the electron beam caused instant CL impulses (not depicted in Fig. 9) that were by 1–2 orders of magnitude more intense than the main quasi-steady CL signal pedestal. The nature of these CL spikes remained unclear. Presumably, they could be caused by the effects of surface roughness on the electron beam focusing and/or some fast processes within the crystal. According to Fig. 9a, the intensity of Cr^{3+} CL increases at the cooling down to 170 K, remains nearly constant until 115 K and significantly decreases at 80–40 K to about half of the maximum intensity, remaining practically constant until 6 K. The same dependence can be obtained after an additional preheating of the sample to 600 K. It has been shown earlier [65] that at ~170 K the electrons, trapped at Cr-ions, are released: $\text{Cr}^+ \rightarrow \text{Cr}^{2+} + e$. However, the main part of Cr^{3+} -centers can be restored only at 330–420 K, when holes are released from various V-type hole centers and recombine with electrons at Cr^{2+} centers.

The obtained results testify that in MgO:Cr SSAFHE indeed provides a considerable contribution to the fast (10^{-3} – 10^{-6} s) component of CL associated with ${}^2\text{T}_1 \rightarrow {}^4\text{A}_2$ and ${}^2\text{E} \rightarrow {}^4\text{A}_2$ radiative transitions in Cr-centers. This is especially apparent in the temperature region of 400–180 K, when the competition with excitons (ionized at such temperatures) is excluded, and Cr^+ centers are unstable. At lower temperatures, however, the situation is more complicated.

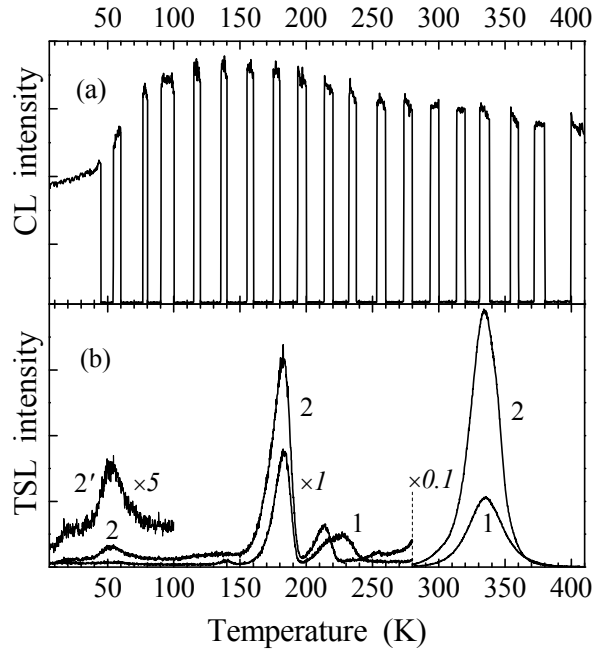


Figure 9. a) The dependence of the CL intensity on the cooling temperature (400 K \rightarrow 6 K) for a MgO:Cr³⁺ (100 ppm) crystal under excitation by 5 keV electrons. (b) The TSL curves measured for 3.4 eV (curve 1) and 3.2 eV emission (curves 2 and 2') in the MgO crystals irradiated by 15 keV electrons at 6 K. The samples were previously annealed at 1575 K (1) or plastically deformed ($\epsilon \approx 4\%$) at 295 K (2, 2'). $\beta = 10$ K/min.

In order to influence the $e-h$ recombination, an MgO crystal was plastically deformed (its thickness decreased by $\epsilon \approx 4\%$) along $\langle 100 \rangle$ at room temperature, introducing a number of structural defects (vacancies, bivalancies, dislocations, inner cavities) into the bulk. Another crystal was annealed at 1575 K for 2 h in an effort to remove dislocations and other structural defects. Both crystals underwent irradiation by electrons under conditions similar to those mentioned above, and then their TSL at 6–400 K (10 K/min) was measured (Fig. 9b). The plastically deformed sample (curve 2) shows a significant enhancement in the TSL peaks at ~ 340 K and 50 K. It is known (see Table 4) that at 335–345 K the release of holes from V_{OH} and V^0 -centers takes place. The peak at 50 K is associated with the release of holes from $[hCa]^{+}$ -centers and their recombination with the electrons trapped at bivalancies (this will be discussed in the next sections), the number of which is increased in the deformed sample.

Electron trapping at low temperatures is in competition with the direct excitation of Cr-centers by hot conduction electrons. This assumption was supported by the fact, that the CL intensity in the deformed sample measured

under the same conditions decreased with T by a factor of ~ 8 compared to ~ 2 in the non-deformed MgO:Cr sample. Therefore, deformation-induced defects serve as efficient centers for electron localization. Electron trapping is not considered to be important from the point of view of non-impact FD creation, because holes in MgO usually carry smaller amounts of energy, so their recombinations with localized electrons yield energies well below E_g , which is not enough to create defects. However, the existence of SSAFHE is important, as it shows that the energy of hot conduction electrons is spent on the excitation of impurity centers. Therefore, the energy of conduction electrons is dissipated via impurity center emission, consequently, reducing the probability of hot $e-h$ recombinations, which are required for the realization of the non-impact FD creation mechanism.

7.2. Bivacancies: charge carrier traps and the source of 2.9 eV emission

The emission of 2.9 eV is quite typical in MgO, and its intensity is known to increase after plastic deformation at room temperature [67]. Therefore, it was associated with the defects created by deformation, but the exact center responsible for the emission and related process remained unclear.

In attempt to solve this problem, the CL (15 kV, 100 nA) spectrum of a highly pure MgO single crystal, plastically deformed along $\langle 100 \rangle$ ($\varepsilon = \sim 4\%$), was measured at 6 K (Fig. 10 insert) [V]. The main CL bands are peaked at 5.2 and 2.9 eV. The excitation spectra of these emissions were also measured at 9 K using synchrotron radiation (curves 1 and 2, respectively). The 5.2 eV emission is excited at ~ 7.6 eV – just below the formation region of large-radius excitons (marked with a double arrow), and the 2.9 eV emission is excited in a wide range of 6.8–7.4 eV.

It was shown on alkali halides [68] that such wide excitation bands arise from bivacancies, which also have different emissions for both cation and anion “edge”. Combining it with the fact, that, according to the Seitz mechanism [69], bivacancies are one of the main defect types introduced into the crystal by deformation, we concluded, that both of the 2.9 and 5.2 eV emissions in MgO are related to bivacancies.

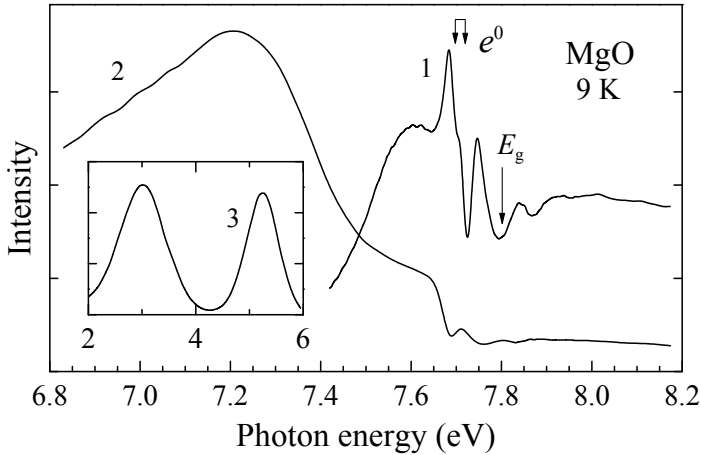
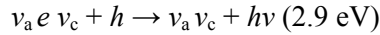


Figure 10. Excitation spectra for 5.2 eV (1) and 2.9 eV (2) emissions measured at 9 K for a plastically deformed MgO crystal. The insert shows CL spectrum (3) of a deformed MgO crystal at 6 K.

Even though bivacancy as a whole is neutrally charged and, therefore, has a small cross-section for interaction with charge carriers, the anion component of a bivacancy is able to capture an electron, which is proven by the existence of a $v_a e v_c$ (P^-) center. As the 2.9 eV emission is peaked in the TSL spectra at temperatures where the release of holes takes place, it is natural to assume that this emission arises from recombination of holes with the electrons trapped at bivacancies:



This is consistent with our empirical observation that in MgO with $E_g \approx 8 \text{ eV}$, the impurity/defect related recombination luminescence with $h\nu < 4 \text{ eV}$ arises mainly due to recombination of mobile holes with localized electrons. On the other hand, luminescence with $h\nu > 4 \text{ eV}$ is caused either by recombination of conduction electrons with trapped holes or by the tunnel recombination between electrons from shallow traps with trapped holes. This latter observation allows assuming that the 5.2 eV emission may arise from recombination of electrons with the holes trapped at the cation component of a bivacancy. However, experimental proof for the existence of a $v_a v_c h$ center is yet to be obtained.

It is also worth mentioning that the 2.9 eV emission is usually enhanced in MgO crystals irradiated with swift heavy ions, which testifies that this type of irradiation causes internal stress and, consequently, forms bivacancies. Bivacancies are formed in the outer track region, and in the track core more complex associates of vacancies are produced.

7.3. Localization of holes near impurities

It is generally accepted that holes in MgO do not undergo self-trapping. However, holes can be easily localized at oxygen ions near cation vacancies (V-center) or at monovalent cations (Li^+ , Na^+). In these cases, holes are trapped mainly by the Coulomb charge of the initial centers, forming electrically neutral centers, which have a rather small cross-section for recombination with hot conduction electrons. More interesting are the cases when holes are localized not by electrostatic attraction, but due to the local deformation potential of the crystalline lattice near isovalent Ca^{2+} and Be^{2+} ions. These centers are similar to self-trapped holes and are positively charged, which gives them a large cross-section for recombination with conduction electrons and, therefore, makes them good candidates for the sites where the non-impact mechanism of FD creation could take place. This was the primary reason for our interest in $[\text{hCa}]^+$ and $[\text{hBe}]^+$ hole centers (Ca^{2+} or Be^{2+} substituting Mg^{2+} next to the hole trapped on an oxygen ion).

The low-temperature irradiation of the MgO single crystals containing purposely introduced impurity hole traps with photons of $h\nu \geq E_g$ (7.8 eV), X-rays or an electron beam causes the formation of electron-hole pairs. Highly mobile valence holes undergo a rapid localization near dominant hole trapping centers, while conduction electrons lose their energy excess down to the bottom of the band via fast vibronic relaxation. Thereupon totally relaxed electrons mainly recombined with the trapped holes. Figure 11 demonstrates the corresponding wide luminescence bands detected via a double VUV monochromator at the excitation of doped MgO single crystals by 10 keV electrons at 10 K. The same luminescence bands have been detected under crystal excitation by SR of 9–30 eV at 6–10 K. The wide emission band peaked at the highest energy of ~ 6.8 eV is related to the electron recombination luminescence in MgO:Ca. The maximum of the recombination luminescence band in MgO:Be is located at a lower energy (~ 6.2 eV [70]). The intensity of both recombination emissions drastically decreases (more than by three orders of magnitude) in ~ 1 s after an electron irradiation is stopped. The continuously weak phosphorescence is typical of the tunnel recombination between spatially separated but trapped electrons and holes.

The MgO:Ca crystals were grown at the Institute of Physics of the University of Tartu. The starting material was a mixture of high-purity (99.9%) MgO and CaCO_3 powders. The mean concentration of the most common metallic impurities was ~ 10 ppm. The concentration of Ca^{2+} in the MgO powder was ~ 10 ppm. To lower the concentration of uncontrolled impurities, the purest parts of the initially grown crystals were used as the starting material for the second growth. The estimated concentration of Ca^{2+} in the final crystals was ~ 200 ppm.

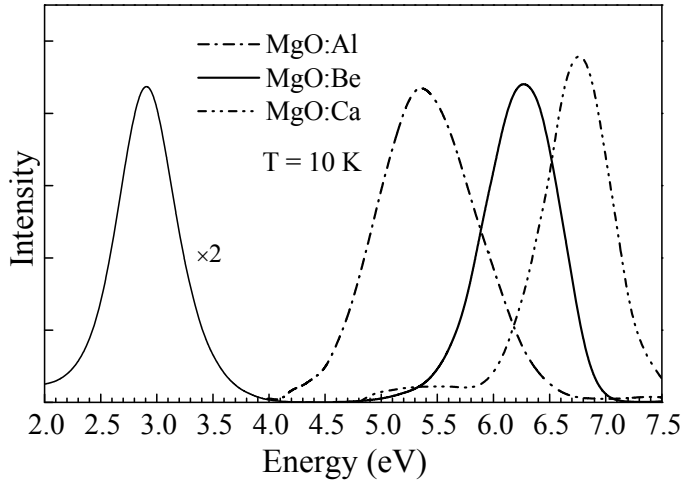


Figure 11. Emission spectra of MgO: Be (solid line), MgO: Al (dashed-dotted line) and MgO:Ca single crystals (dashed-double-dotted line) under the excitation by 10-keV electrons at 10 K

In MgO, Ca^{2+} impurity ions replace regular cations and form substitutional solid solutions with the concentration of calcium ions of up to several at%. The ionic radius of Ca^{2+} surrounded by six O^{2-} is larger than that for Mg^{2+} (1.14 Å and 0.86 Å, respectively). So, the doping of MgO with Ca^{2+} causes the expansion of the crystal lattice. It is obvious that the Ca^{2+} situated at cation lattice sites cannot serve as traps for conduction electrons because the ionization energy E_i of a free Ca^+ is about 3 eV lower than of Mg^+ .

In [71], a 6.8 eV luminescence peak was reported in Ca-doped MgO crystals and assigned presumably to a $[\text{hCa}]^+$ center. To verify this conclusion, which was in contradiction with the assignment of the ~6.9 eV emission in nominally pure MgO to self-trapped excitons [40], additional investigations of MgO:Ca (~200 ppm) were performed in our laboratory. According to [72], a quasiline emission of free excitons at 7.69–7.70 eV dominates in the photoluminescence spectrum of highly pure MgO, while the emission band peaked at 6.8 eV is absent. On the other hand, quasiline emission at 7.65 eV (i.e. shifted toward low-energy region with respect to the emission of free excitons) and intense broadband emission peaked at 6.8 eV were detected in MgO:Ca crystals. The intensity of broadband emission decreases parallel to the decrease in the concentration of calcium impurity ions. The 6.8 eV luminescence is efficiently excited by synchrotron radiation of 7–40 eV, i.e. both below the edge of fundamental absorption and at the formation of free excitons or separated electrons and holes (band-to-band transitions) [73]. The efficiency of the 6.8 eV emission is especially high at 25–30 eV, where the values of the absorption constant are relatively low, thus, decreasing the outcome of conduction electrons and

valence holes at the surface. In addition, the multiplication of $e-h$ pairs, when one exciting photon forms two or even more $e-h$ pairs, if the photon energy exceeds ~ 24 eV [73, 74].

Fig. 12 demonstrates the temperature dependences of the luminescence intensity measured for the quasiline emission at 7.65 eV and broadband emission with the maximum at 6.8 eV (band width of ~ 0.8 eV, measurement was performed at 7.1 eV) at the steady excitation of MgO:Ca by SR of 25 eV [III], which selectively forms separated electrons and holes. The absorption constant at 25 eV is significantly lower, than at the beginning of band-to-band transitions, and the 25 eV photons excite crystal regions located rather far from the surface. The thermal quenching of the emissions starts above ~ 40 K, and the intensities are decreased by half at about 50 K. To elucidate the processes responsible for the thermal quenching, the TSL has been measured after irradiation of MgO:Ca by X-rays (50 kV, penetration depths exceeds the thickness of our sample) at 6 K. The TSL was measured for 2.9 eV emission with the heating rate of $\beta = 10$ K/min. The 48 K TSL peak is dominant for 2.9 eV emission, while a weak TSL peak at ~ 36 K is most notice able for ultraviolet emission. The TSL has been detected on the background of a weak temperature-independent (8–80 K) tunnel phosphorescence with a complex spectral composition. A similar TSL curve ($\beta = 10$ K/min) has been detected in MgO:Ca previously irradiated by 6-keV electrons at 6 K. The analysis of the dependences of steady photoluminescence on temperature and the TSL curves testify that $[hCa]^+$ centers are formed after irradiation of MgO:Ca, resulting in the hole trapping by Ca^{2+} impurity ions located at regular cation sites. The thermal ionization of $[hCa]^+$ centers takes place at about 50 K. The hole delocalization causes a sharp attenuation of the 6.8 eV emission, when the holes released from $[hCa]^+$ centers migrate to still localized (for example, at bivanancies) electrons. The latter recombination process manifests itself in the TSL peak at ~ 48 K in previously irradiated MgO:Ca: thermally released holes recombine with the localized electrons with the 2.9 eV emission.

MgO:Be single crystals were grown at our Institute of Physics, Tartu. The mean concentration of the most common metallic impurities was ~ 10 ppm, and the estimated concentration of Be was approximately 150 ppm. Doping of MgO single crystals with Be results in the formation of a number Be-containing centers [70]. The $[hBe]^+$ center ($Be^{2+}-O^-$) is created by X-irradiation at 77 K, its EPR spectrum is best observed at 4 K and high microwave powers. It has a tetragonal symmetry with a slight orthorhombic distortion. This distortion is caused by the off-center position of the small Be^{2+} ion (the ionic radius equals 0.41 Å and 0.3 Å for 4- and 3-coordination, respectively) in an Mg^{2+} cation site. The $[hBe]^+$ hole center does not have any obvious Coulomb precursor for the hole trap. However, due to the small ionic radius, the Be^{2+} that substitutes for regular Mg^{2+} cation, is hopping inside the cation vacancy site, polarizing the surrounding oxygen ions. When MgO:Be is subjected to irradiation, such polarization acts as a shallow trap for holes. At some point, when a hole

localizes at the O^{2-} neighboring the Be^{2+} , the latter relaxes away from the former, hence, the potential well is deepened, so that its depth is sufficient for localizing the hole and formation of a Be^{2+} trapped-hole center. The value of E_i for Be^+ is by ~ 3 eV higher than that for Mg^+ and, in principle, electrons can also be trapped at Be^{2+} . However, the effective cross-section of electron trapping by Be^{2+} is at least by dozens of times lower than the effective cross-section for the recombination with the Coulomb centers formed at hole trapping nearby Be^{2+} ions.

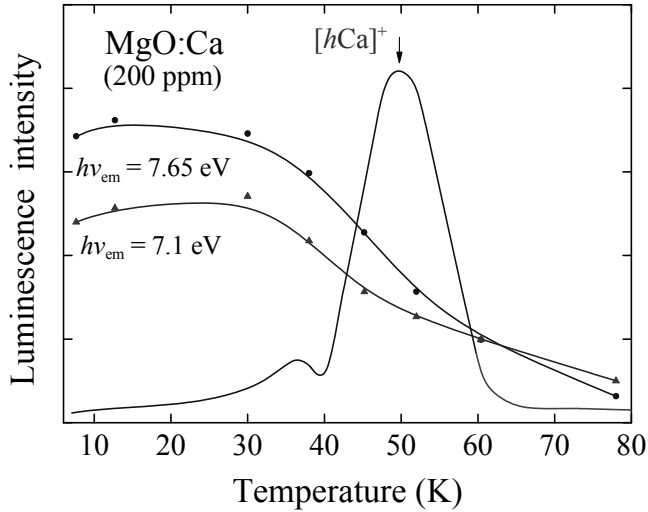


Figure 12. The temperature dependences of the steady luminescence intensity measured for quasiline emission at 7.65 eV (•••) and broadband emission at 7.1 eV (▲▲▲) at the excitation of MgO:Ca by synchrotron radiation of 25 eV and the TSL curve (solid line) measured after irradiation of MgO:Ca by X-rays at 6 K ($\beta = 10$ K/min).

The heating of an X-irradiated MgO:Be crystal with a constant rate of $\beta = 10$ K/min from 10 K to $T \geq 190$ K causes the destruction of $[hBe]^+$ centers via hole release and restoration of Be^{2+} at cation sites. The released holes recombine with the electrons still localized at different defect/impurity centers, for instance, with the appearance of the 2.9 eV emission. Some holes are also localized at deeper traps, for instance, V_{Al} centers in $MgO:Al^{3+}$ are stable up to 375 K [75].

Figure 13 shows the thermoactivation characteristics of MgO:Be²⁺ (150 ppm) single crystals [III]. The pulse annealing of the EPR signal of $[hBe]^+$ centers was measured in the sample X-irradiated at 10 K. The TSL curve ($\beta = 10$ K/min) was measured for 2.9 eV emission in an MgO:Be²⁺ crystal irradiated for 1 hour by 5 keV electrons at 5.2 K. The main TSL peak at ~ 190 K accompanies a sharp decrease of the EPR signal intensity. The thermal

quenching of the 6.2 eV emission (under excitation by 25 eV photons), connected with the release of electrons from some traps and their recombination with the holes from $[h\text{Be}]^+$ centers, takes place in the same temperature region. So, there is no doubt that we have a hole process at about 190 K.

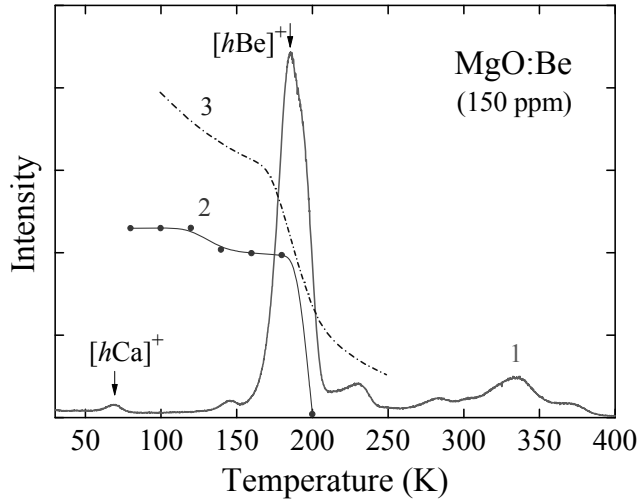


Figure 13. Thermoactivation characteristics of $\text{MgO}:\text{Be}^{2+}$ (150 ppm) single crystals. TSL of 2.9 eV (curve 1) for sample irradiated for 1 hour by 5 keV electrons at 5.2 K. The annealing of the EPR signal of $[h\text{Be}]^+$ -centers in the sample X-irradiated at 10 K (curve 2) and the temperature dependence of 6.2 eV emission under excitation by 25 eV photons (curve 3).

The cross-section for the recombination of electrons with charged (Coulomb) $[h\text{Be}]^+$ and $[h\text{Ca}]^+$ centers is at least two orders of magnitude as high as that for neutral trapped-hole centers. In MgO, the energy released at the recombination of a cold electron (relaxed down to the bottom of the conduction band) with $[h\text{Be}]^+$ and $[h\text{Ca}]^+$ is not sufficient for the creation of a pair of Frenkel defects ($E_{\text{FD}} > E_g$). However, non-relaxed (hot) conduction electrons participate in the recombination with $[h\text{Be}]^+$ and $[h\text{Ca}]^+$ as well, in principle, providing conditions for the formation of Frenkel defects. Such hot recombinations are in competition with the multiplication process of $e-h$ pairs, when a sufficiently hot conduction electron (or a hot valence hole) is able to create a secondary $e-h$ pair (see, e.g., [74]). In MgO, the width of the valence band is about 6 eV [76], and hot valence holes do not cause the multiplication of $e-h$ pairs. According to detailed experimental investigations, the efficient creation of secondary $e-h$ pairs occurs, if the energy of exciting photons is $h\nu \approx 25\text{--}30$ eV. So, in the crystal bulk, the energy of non-relaxed conduction electrons, which can be involved in hot recombination instead of the multiplication process, is limited by about 11–16 eV. The energy released at the recombination of such electrons

with $[h\text{Be}]^+$ and $[h\text{Ca}]^+$ centers ranges up to 19–24 eV or even more, i.e. it might be sufficient for the non-impact creation of Frenkel pairs near $[h\text{Be}]^+$ or $[h\text{Ca}]^+$.

Besides $[h\text{Ca}]^+$ and $[h\text{Be}]^+$ centers, another possibility for hole trapping resulting in a positively charged center should be considered. In MgO, the excessive charge of trivalent ions is compensated for by cation vacancies, and these vacancies are often located near the ions they are compensating for, giving rise to linear V_{Me} centers ($\text{Me}^{3+}\text{O}^{2-}v_{\text{c}}h$). If the concentration of a metallic impurity is increased, the probability of two neighboring impurity cations is also increased, leading to the appearance of metallic pairs, which can also be associated with v_{c} ; in this case, the whole center is electrostatically neutral. If this pair center is linear along $\langle 100 \rangle$ ($\text{Me}^{3+}\text{O}^{2-}v_{\text{c}}\text{O}^{2-}\text{Me}^{3+}$), so that the vacancy is situated between impurity ions, then its charge is balanced by those ions, and the vacancy is not attractive for a hole. However, if the structure is not linear, it will have a dipole moment, and a hole may become localized in the negative field of v_{c} , so the center as a whole is no longer neutral, but positive, which, in turn, considerably increases its cross-section for recombination with conduction electrons. So far there is no direct experimental proof of centers with such structure and realization of the described process, although in $\text{MgO}:\text{Cr}^{3+}$, the existence of pair centers in association with a cation vacancy in both tetragonal and rhombic configurations has been proposed [77].

It should be emphasized that the efficiency of hot $e-h$ recombination with creation of Frenkel defects is low in the case of irradiation, which does not provide a high density of electronic excitations, because there is a strong competition with the multiplication of EE and other channels of relaxation. Our experiment with irradiation of an $\text{MgO}:\text{Be}^{2+}$ single crystal by synchrotron radiation ($h\nu = 20$ eV) at 9 K for 3 hours did not yield any detectable signs of increased 2.6 eV absorption of $F_{\text{A}}(\text{Be})$ (near-Be F-centers found after irradiation with heavy ions and described in [83]), which, theoretically, could be created, if the non-impact FD creation mechanism takes place at the recombination of a hot electron with a $[h\text{Be}]^+$ center. However, in the case of an extremely high density of EE achieved under irradiation with swift heavy ions, the probability of such recombination is much higher and should be taken into account.

7.4. The effect of swift heavy ions

Swift heavy ions are able to create Frenkel defects via impact mechanism. However, only a few percents of their initial energy is spent in elastic collisions with ions of the host material, and the remaining energy is spent on the excitation of the electronic system. The density of these excitations is extremely high and cannot be achieved with electromagnetic or neutron irradiation. Therefore, SHI provide especially favorable conditions for non-impact creation of defects and create more complex associates of FD than other types of radiation.

Fig. 14a presents the TSL curves measured at 300–810 K for two MgO:Be single crystals irradiated with 2.5 GeV ^{238}U ions (10^{12} ions/cm 2 , RT) [VI]. Before ion-irradiation, one of these identical samples was additionally exposed to the plastic stress ($\sim 4\%$). In the sample exposed to the plastic stress, there is a significant enhancement of the TSL peaks at 350–480 K measured through an optical filter, the transparency region of which (2.8–4.1 eV) covers the emissions of F^+ centers and oxygen ions nearby $\nu_a\nu_c$. According to EPR investigations (see, e.g., [III]), these peaks are related to the release of holes from the centers that also contain ν_c (peak at 420 K) or ν_c and OH^- ions (peak at 360 K). Fig. 14b presents the TSL of the same two MgO:Be samples measured through an optical filter and a special glass, that additionally transforms the Be-related emission at 6.2 eV into orange light. Although the 6.2 eV emission at high temperatures is relatively weak, there is a clear increase in the intensity of the TSL at 760–810 K in the sample exposed to the plastic stress and subsequent irradiation with SHI.

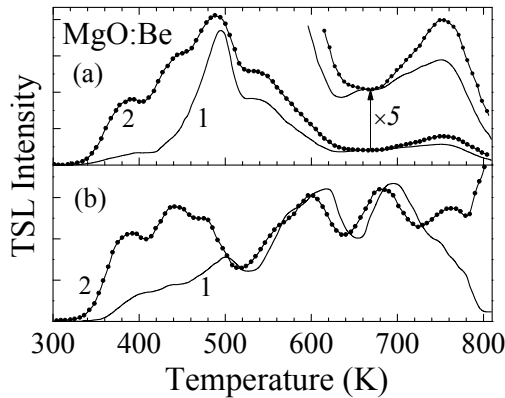


Figure 14. TSL curves (1, 2) measured for two MgO:Be single crystals irradiated with 2.5 GeV ^{238}U ions (10^{12} ions/cm 2 , RT). Before ion-irradiation one sample (curves 2) was additionally exposed to plastic stress ($\sim 4\%$, RT). The TSL were registered through an optical filter (2.8–4.1 eV, part (a)) or the same filter and a glass spectral transformer (b). $\beta = 2$ K/s.

The irradiation with SHI induces the deformation of a crystal, leads to the disordering of a regular lattice and accelerates ionic diffusion along weakened (reduced-symmetry) lattice sites. So, the appearance of the TSL peak at ~ 800 K in the stressed MgO:Be can be tentatively ascribed to the diffusion of interstitials along reduced-symmetry sites of a deformed lattice.

7.5. Irradiation effects in MgO:Cr

Introducing Cr-ions into the MgO lattice leads to the formation of impurity centers with different structures, which were studied by means of EPR, optical polarization methods, applied magnetic fields and elastic uniaxial stress [77–79]. The simplest center is a single Cr^{3+} , which replaces Mg^{2+} and is situated at a site with cubic symmetry. If a cation vacancy, which compensates for the excessive positive charge, is located nearby, it lowers the center's symmetry to tetragonal (Cr-O-v_c along $\langle 100 \rangle$) or rhombic (Cr-v_c along $\langle 110 \rangle$). An increase in the Cr concentration leads to the formation of Cr pairs with the same symmetry. The scheme of these Cr-vacancy centers is depicted in Figure 15.

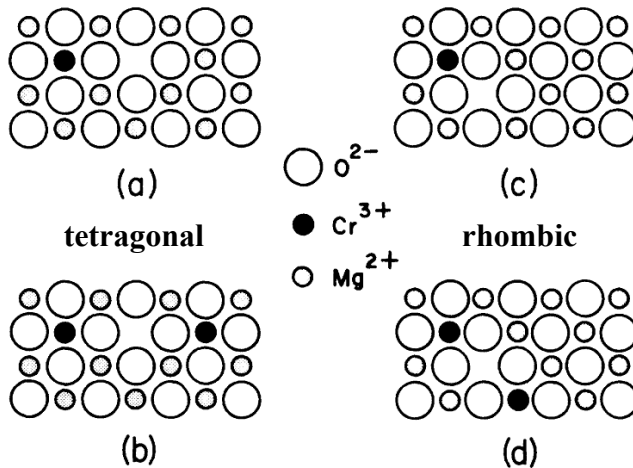


Figure 15. Scheme of noncubic Cr sites in MgO: single (a, c) and pair (b, d) Cr-centers in tetragonal [100] (a, b) or rhombic [110] (c, d) symmetry.

The radiative transition ${}^2E \rightarrow {}^4A_2$ in cubic and tetragonal centers causes a series of characteristic zero-phonon lines and their broader phonon sidebands in the region of 1.78–1.65 eV (698–750 nm). As the vacancy in a tetragonal center is situated around oxygen ion, the perturbation of Cr is not very strong, and the emission is similar to that of cubic centers with a slight shift to lower energies. For the same reason, it is difficult to distinguish between emissions of single and pair tetragonal centers: the interaction of Cr ions in the $\text{Cr-O-v}_c\text{-O-Cr}$ chain is very weak. The lifetimes of cubic and tetragonal centers are also very close: 11.6 and 8.6 ns at 77 K, respectively. The situation is different in rhombic centers, where the vacancy is closer to the Cr-ion and, therefore, its perturbing influence is stronger: the broadband emission associated with these centers lies in the region of $\sim 1.77\text{--}1.24$ eV (700–1000 nm) with the maximum at ~ 1.55 eV (800 nm) and has the lifetime of 35 μs . The positions of Cr-related lines and

related centers are summarized in Table 6, according to [79]. It should be noted, however, that the exact position of the emission lines slightly varies, depending on the crystal growth conditions [78].

Table 6. Emission of various Cr-centers in MgO:Cr³⁺ at 77 K according to [79].

Emission		Center symmetry	Center orientation	Transition	Line nature
nm	eV				
698.1	1.776	Cubic		${}^2E \rightarrow {}^4A_2$	0-phonon line (R-line)
698.9	1.774	Cr- v_c -Cr ?	[001]	${}^2E \rightarrow {}^4A_2$	0-phonon line
699.2	1.773	tetragonal	[001]	${}^2E \rightarrow {}^4A_2$	0-phonon line
703.5	1.762	Cr- v_c -Cr ?	[001]	${}^2E \rightarrow {}^4A_2$	0-phonon line (N1-line)
703.8	1.762	tetragonal	[001]	${}^2E \rightarrow {}^4A_2$	0-phonon line (N2-line)
708.2	1.751	rhombic	[011]		
708.6	1.750	rhombic	[011]		
711	1.744				R-line acoustic sideband
718	1.727				R-line major optical sideband
719	1.724				N-lines acoustic sideband
725	1.710				N-lines major optical sideband
741	1.673				R-line minor optical sideband
749	1.655				N-lines minor optical sideband

In our experiments, we used Cr-centers as luminescent probes for energy and charge transfer processes. Related luminescence spectra were recorded at 9–10 K with a CCD detector using SR for excitation. Unfortunately, the entrance slit width of 0.1 mm did not provide high resolution, so the emission of close zero-phonon lines of tetragonal centers was observed as one peak.

Figure 16a from the classical study [80] shows the spectrum of the imaginary part of the complex permittivity ϵ_2 for the long-wavelength part of MgO fundamental absorption at 25 K. The onset of interband transitions with the generation of separated electrons and holes is indicated: $E_g = 7.783$ eV. Hydrogen-like excitons with $n = 1, 2, 3$ and an inverse (in comparison with alkali halide crystals) location of singlet and triplet excitons on the energy scale are formed at lower energies [72]. The lower states in alkali halides are long-lived triplet states; this circumstance facilitates exciton self-trapping. When the fast luminescence of singlet excitons, which are highly mobile and do not undergo self-trapping in regular lattice regions, was revealed in the CL and PL spectra of MgO, it became evident that a lower energy is necessary to form short-lived singlet excitons in MgO. Figure 16a also shows the luminescence spectrum of free excitons (measured by Feldbach and Kuusmann, Tartu), which is described by a Lorentzian and shifted by ~ 10 meV with respect to the absorption spectrum of singlet excitons.

Nominally pure MgO single crystals contained (according to the ESR data) less than 5 ppm of Cr³⁺ ions. The CCD spectra at the excitation, which

selectively forms different exciton states or separate e and h , were recorded at 9 K (Fig. 16b) [IV]. The shape of all of these spectra is almost the same as in the case, when 7.69 eV excitation photons form the lowest singlet state of exciton. This shows, that the effective energy transfer to cubic and tetragonal centers takes place via both excitons and $e-h$ pairs.

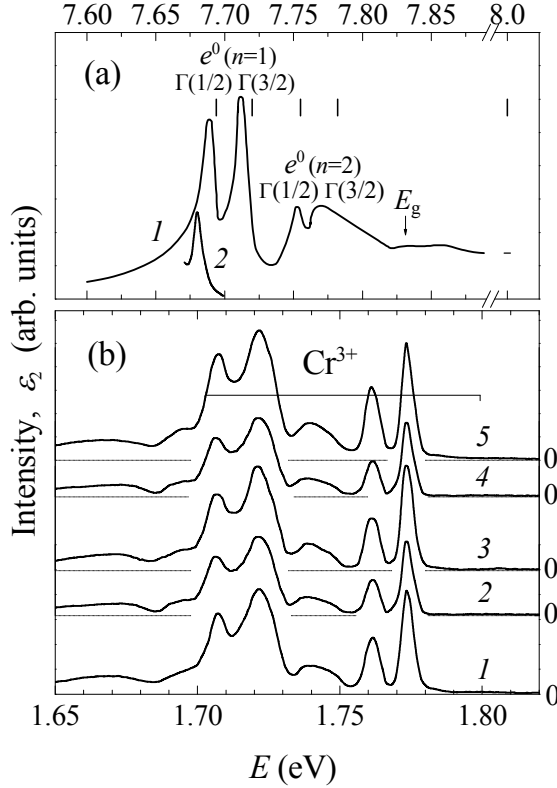


Figure 16. (a) Spectra of ε_2 (1) at 25 K [80] and free exciton emission at 9 K (2) for MgO single crystals. Energies of excitation photons indicated in panel (b) are primed. (b) Emission spectra of Cr^{3+} centers in nominally pure MgO upon excitation by synchrotron radiation with photon energies of 7.694 (1), 7.72 (2), 7.775 (3), 7.782 (4), and 8.00 eV (5), recorded at 9 K using a nitrogen-cooled CCD detector.

Basing on this result, a wider range of excitation energies (4–32 eV) was investigated at 9 K using SR for $\text{MgO}:\text{Cr}^{3+}$ crystals with an estimated concentration of Cr \sim 100 and \sim 850 ppm. These crystals were previously studied by EPR and laser spectroscopy methods [III, 81]. Particular attention has been given to the role of pair chromium centers in the creation of radiation defects. Although chromium as a luminescent center seems to dissipate the energy of hot conduction electrons, lowering the probability of hot $e-h$ recombination (see

Section 7.1), we assumed that a very high Cr^{3+} concentration (~ 850 ppm), on the contrary, causes the decrease of radiation resistance due to the localization of holes at complex chromium centers and subsequent hot $e-h$ recombination with the creation of FD. A hole could be trapped by a linear tetragonal pair chromium center or by a rhombic pair chromium center (RPCC, different from the structure of Fig. 15d), where two Cr^{3+} are located in two cation rows perpendicular to each other, while one of the oxygen ions in an anion row is shifted closer to the cation vacancy (Fig. 17). In both cases, one cation vacancy serves as a charge compensator for two trivalent impurity ions. A Coulomb center with a large recombination cross-section is formed after hole trapping by a RPCC at the oxygen ion nearest to v_c , and the energy released at the recombination of a hot electron with such Coulomb trapped-hole center could be sufficient for both excitation of Cr^{3+} -center emission and for the non-impact creation of a stable FD pair. It is important, that an anion vacancy and oxygen interstitial are formed within an anion row (features of RPCC microstructure!), which facilitates a crowdion displacement of an interstitial from a birthplace along the $[110]$ direction.

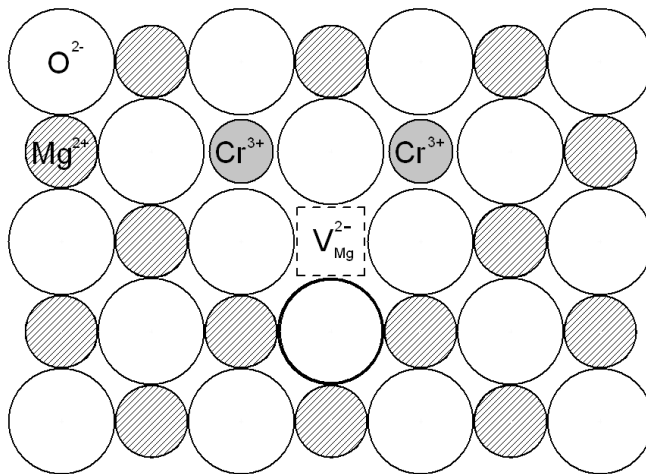


Figure 17. Scheme of a possible rhombic pair chromium center in MgO which would favor hole trapping. The oxygen ion shifted to the vacancy is marked with bold line. Numbers show the effective charge of centers relative to the lattice, assuming that Cr are in the 3+ state.

Another possibility is the realization of defect creation via collapse of solitons [8, 9]. Cr-ions in the model (Fig. 17) are located very close to each other, with a combined mass $54 + 54 = 108$, which is 6.5 times greater than the mass of the oxygen with captured hole. Therefore, this cluster might provide the conditions for very unharmonic oscillations, which may relax not via the creation of

elementary Frenkel defects, but via a rearrangement of large ion clusters, resulting in complex 3D defects. The energy required for such process could be provided by recombination of trapped holes with highly energetic (100–300 eV) electrons, which are produced in Auger-processes (involving core shells) occurring under irradiation with X-rays or keV-electrons. This relaxation channel should lower the quantum efficiency of RPCC emission compared to the light ($27 + 27 = 54$) Al^{3+} -based analogue pair centers under the same excitation. In any case, it appears that vacancy-compensated heavy impurity pair centers lower the radiation resistance of MgO. The opposite effect is expected for the pairs of isovalent luminescent ions ($\text{Ni}^{2+}\text{-Ni}^{2+}$), which do not require a vacancy for charge compensation and are likely to have an increased luminescence efficiency (luminescent protection!). The investigation of such centers lies ahead.

Our measurements included recording excitation spectra for Cr^{3+} -related emission using energies 4–20 and, in particular, 20–34 eV. For these energies, the emission spectra at certain points were also measured with the CCD detector in the region of 1.85–1.38 eV (690–900 nm). The equipment parameters were: ARC monochromator, grating 300/500, slit 0.1, filter GG420 in the emission channel, CCD accumulation – twenty 5-second impulses (100 s). An example of such CCD spectrum is presented in Fig. 18. Besides zero-phonon lines and sidebands of cubic and tetragonal centers, the measured region includes a non-elementary broadband emission (bandwidth of ~ 0.25 eV) peaking at ~ 1.6 eV, which is related to rhombic (single and pair) chromium centers.

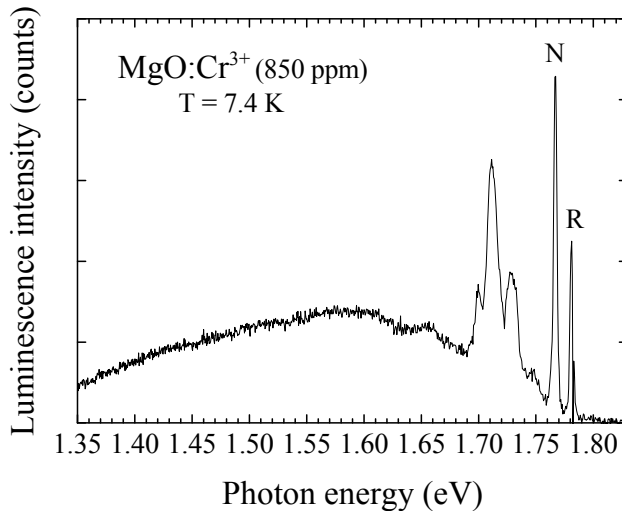


Figure 18. CCD emission spectrum for X-irradiated $\text{MgO}:\text{Cr}^{3+}$ (850 ppm) single crystal for excitation 5.9 eV (210 nm) at 7.4 K. No-phonon lines of cubic and tetragonal centers are marked with R and N letters, respectively.

Fig. 19 presents the excitation spectra for the emissions of cubic and tetragonal Cr^{3+} centers (R- and N-line, respectively) in an $\text{MgO}:\text{Cr}^{3+}$ (850 ppm) crystal at 9 K [VII]. The excitation spectra were constructed on the basis of a set of the CCD emission spectra recorded at varying energies of the exciting photons from 4 to 32 eV (the underlying base of the broad-band emission was subtracted from the emission intensities of lines and their sidebands). According to our data, a preliminary irradiation of $\text{MgO}:\text{Cr}^{3+}$ with X-rays at room temperature (55 kV, 15 mA, 2 h) significantly changes the excitation spectra for the N- and R-lines of Cr^{3+} -center emission at subsequent measurement using synchrotron radiation at 9 K. In an X-irradiated crystal, the efficiency of R- and N-emissions is halved in the region of intracenter excitation by $h\nu = 5.5\text{--}7.5$ eV photons, while the rise of $h\nu$ from 24 to 32 eV causes an increase in the efficiency of the R- and N-lines by a factor of 5 or 3, respectively (see Fig. 19). Up to now, the rise of the Cr^{3+} -emission efficiency at 24–32 eV was interpreted as a result of either allowed intracenter (chromium-oxygen complexes) transitions up to highly excited states [82] or the multiplication of EE, when one exciting photon creates three to four $e\text{-}h$ pairs, each of which transfers its energy to Cr^{3+} centers [74]. A detailed analysis of the obtained data allows concluding, that the contribution of both abovementioned processes should be taken into account.

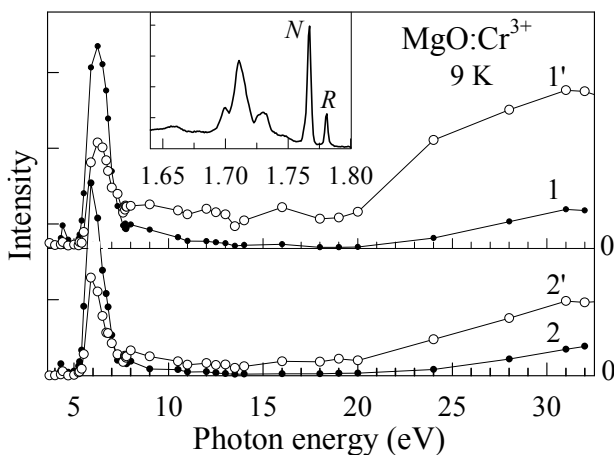


Figure 19. Excitation spectra of tetragonal (1, 1') and cubic (2, 2') Cr^{3+} -center emission in $\text{MgO}:\text{Cr}^{3+}$ (~850 ppm) single crystals, non-irradiated (1, 2) or preliminary irradiated with X-rays (1', 2). The insert shows a typical CCD spectrum at 9 K used to obtain excitation spectra points (in particular case, an intracenter excitation with the 6.5 eV photons).

Non-elementary broad-band emission demonstrated a clear component at ~ 1.42 eV at the lowest excitation energies (3.7–5 eV), especially in the X-irradiated sample, so the excitation spectra of the broad-band emission were

constructed using the aforementioned method for both (1.6 and 1.42 eV) points. The resulting spectra are presented in Fig. 20. The enhancing influence of X-rays on the excitation efficiency above E_g is the same as in the case of cubic and tetragonal centers. Below 7 eV, the spectra ratio for non-irradiated and X-irradiated samples is more complicated. While the 1.42 eV component looks enhanced in the X-irradiated sample, little to no change is observed for the main 1.6 eV component. However, as absolute emission intensity values were taken for construction, the width and overlapping of these components should be taken into account. According to Fig. 18, it is most likely that for both 1.42 and 1.6 eV points of the broad emission band we have a sum of two or maybe even more overlapping components, so their individual excitation efficiencies are not clear. Nevertheless, the excitation energy of ~ 5 eV seems particularly interesting, as for both non-irradiated and X-irradiated samples, at this excitation lines related to cubic and tetragonal centers, which started to emerge below ~ 4.5 eV, are absent and appear again only above ~ 5.25 eV, while the broadband emission, apparently, undergoes an intensity shift from 1.42 eV to 1.6 eV. It is possible that these components are related to the same (probably chromium-pair) centers with different charge state, which changes at ~ 5 eV – the energy, which coincides with the excited state of F-centers, so a tunnel transfer of an electron from an excited F-center to a rhombic center might take place.

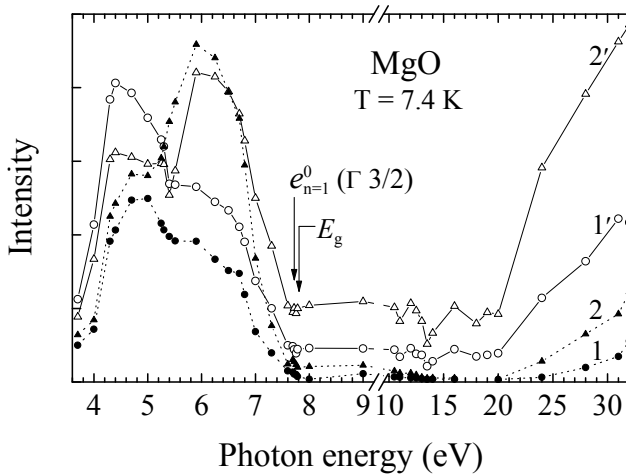


Figure 20. Excitation spectra for 1.42 eV (1, 1') and 1.6 eV (2, 2') components of broad-band emission related to rhombic centers in MgO:Cr³⁺ (~850 ppm) single crystals, non-irradiated (1, 2) or preliminary irradiated with X-rays (1', 2').

A preliminary analysis of our latest similar experiments on MgO:Cr³⁺ (100 ppm) demonstrated the same enhancing effect of X-irradiation on the emission of cubic and tetragonal centers (broad-band luminescence is absent at this concentration). However, exposure to energies of 16–19 eV lead to an overall decrease in the luminescence intensity and changes in relative intensity of R and N lines. This difference was noted, when a CCD spectrum at the excitation energy of 16 eV was taken again after measuring several spectra in the region of 16–19 eV.

The influence of X-rays on Cr-doped MgO may be explained as follows. Irradiation with X-rays produces mobile electrons and holes. At room temperature, holes become trapped on some still stable hole centers, and electrons become trapped on Cr³⁺ centers, converting them into Cr²⁺, which are stable at RT and remain in this charge state after cooling down to 9 K. However, cubic and tetragonal Cr-centers containing Cr²⁺ do not produce the characteristic Cr³⁺ emission. Therefore, they are effectively excluded from the emission spectra measured at excitation energies below E_g , and the efficiency of excitation is lower in the X-irradiated sample, as is observed in Fig. 19. The situation changes, if the excitation energy exceeds E_g , and mobile charge carriers are created. Valence holes reach Cr²⁺ centers and recombine with electrons there, creating excited Cr³⁺ centers, which relax with a characteristic emission, and the overall efficiency of excitation is higher in the region, where $e-h$ pairs are created (8–20 eV), and it increases even more at excitation above 20 eV, where multiplication of EE takes place. In the case of samples that were not irradiated with X-rays, most Cr ions at 9 K are still in the 3+ state. The conduction electrons produced by $h\nu > E_g$, have to become trapped at Cr³⁺ first, so the excitation efficiency is lower compared to the X-irradiated sample.

As irradiation with SR at $h\nu > E_g$ constantly produces $e-h$ pairs, after some period both X-irradiated and non-irradiated samples should arrive at the same equilibrium point, where the excitation efficiency is determined by the probability of electron capture at Cr³⁺ and consequent recombination with a hole. This assumption explains the aforementioned decrease in the excitation efficiency and changes in the R- and N-line intensities of X-irradiated MgO:Cr (100 ppm) at $h\nu = 16$ eV. This behavior was not observed under similar conditions in the sample with Cr concentration of 850 ppm, most likely due to the larger total concentration of centers and larger fraction of pair tetragonal, single rhombic, and pair rhombic centers, which may act differently from cubic and single tetragonal centers abundant in the samples with a lower concentration.

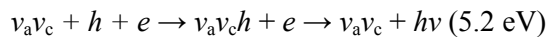
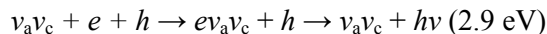
SUMMARY

The main investigation objects were highly pure and doped NaCl and MgO single crystals grown at the Institute of Physics, Tartu. The crystals have the same face-center cubic structure and close values of the energy gap (about 8.8 and 7.8 eV in NaCl and MgO, respectively), but very different melting points (1074 and ~ 3200 K) and a specific behavior of holes and excitons. The formation energy of a Frenkel pair exceeds the energy gap in both, NaCl (at $T < 120$ K) and MgO, crystals: $E_{\text{FD}} > E_{\text{g}}$. A comparative complex study of the radiation resistance of these materials, as well as the elementary creation mechanisms of Frenkel defects and their stable associations by 6–40 eV photons, X-rays (~ 50 keV), electrons (4–20 keV), and swift heavy ions (SHI: ^{198}Au , ^{238}U , $\sim \text{GeV}$, for MgO)), has been performed using the methods of optical and thermoactivation spectroscopy in a wide temperature region (6–875 K). The main results on the creation mechanisms of nanosize radiation defects and the prospects to influence the efficiency of radiation damage in wide-gap dielectrics are the following:

1. Using a highly sensitive luminescent method, the creation spectrum of long-lived ($\tau > 1$ s) pairs of anion Frenkel defects (F-H pairs with interdefect distance of several lattice constants) by VUV radiation of 7–40 eV at 12 K has been measured for a highly pure NaCl single crystal, that demonstrates a rather high resistance against irradiation at low temperatures ($E_{\text{FD}} > E_{\text{g}}$). It is confirmed that the efficiency of long-lived FD creation (η_{FH}) via the decay of self-trapped excitons or the recombination of relaxed electrons with self-trapped holes is very low, while a sharp rise of η_{FH} is revealed at 12–16 eV, where an exciting photon is not able yet to provide multiplication processes, but forms a hot $e-h$ pair, and the energy released at the recombination of a such pair exceeds E_{FD} . The efficiency of F-H pair creation doubles, when an exciting photon of 28–32 eV forms already two hot $e-h$ pairs, while η_{FH} sharply decreases at the photocreation of cation excitons (~ 33 –34 eV). A hopping diffusion of H centers starts above 30 K and is accompanied by the annealing of their EPR signal and appearance of the TSL peak at about 35 K, which consists mainly of the 3.4 eV emission of triplet self-trapped excitons. In our opinion, this emission tentatively results from the recombination between H and F centers from a close F-H pair via the excited state of STE (“radiative assembly of an STE”).
2. Heating of NaCl above 120 K leads to anharmonic expansion of a crystal lattice, and the value of E_{FD} decreases ($E_{\text{FD}} < E_{\text{g}}$), thus, facilitating FD creation at high temperatures. At the same time, the contribution of hot carriers to the creation of F-H pairs and their associations in crystal bulk has been demonstrated by a direct absorption method in highly pure NaCl and KCl crystals irradiated in the two-photon absorption mode (crystals uniformly colored in 1–3 mm-thickness) at RT. Irradiation with a KrF excimer

laser ($2 \times 4.99 \text{ eV} = 9.98 \text{ eV}$) causes mainly the formation of cold (relaxed) $e-h$ pairs, while ArF-irradiation ($2 \times 6.42 \text{ eV} = 12.84 \text{ eV}$) produces already hot and spatially separated e and h . The presence of highly mobile hot valence holes sharply increases the creation efficiency of temperature-stable defect associations – F_2 centers and X_3^- trihalide centers – in the crystal volume.

3. The manifestations of a solid-state analogue of the Franck-Hertz effect (SSAFHE) – direct excitation of impurity ions by hot conduction electrons, the energy of which is still insufficient for the creation of secondary excitons or $e-h$ pairs, has been revealed in the photo- and cathodoluminescence of doped NaCl and MgO crystals. In alkali halides (for instance, NaCl:TI⁺), the SSAFHE can be considered as a luminescent protection against nonimpact mechanisms of FD creation, when a hot conduction e loses a part of its energy via SSAFHE (i.e. radiative channel), thus decreasing the FD creation efficiency at a subsequent recombination of a “cooled” e with an h . However, the influence of SSAFHE on the radiation resistance of MgO:Cr³⁺ is significantly lower, because nonimpact $E_{FD} \approx 30 \text{ eV}$, and it is rather difficult to provide the formation of sufficiently hot $e-h$ pairs because of a competition with the $e-h$ multiplication processes.
4. A set of impurity-related shallow hole traps – in particular, Ca²⁺ and Be²⁺ ions – have been revealed in MgO crystals, where neither electrons and holes, nor large-radius excitons undergo self-trapping. These impurity ions are isovalent with Mg²⁺ cations, and the holes are trapped at neighboring oxygen ions mainly due to a local lattice deformation. A trapped-hole center possesses a positive electric charge with respect to a regular lattice ($[hCa]^+$, $[hBe]^+$) and a large cross-section for the recombination with hot conduction e , thus, providing favorable conditions for non-impact creation of FD. This is true even for temperatures above ionization of these centers, as holes could still get trapped for a short time. The result demonstrates the importance of purification of MgO from certain impurities in order to increase its radiation resistance.
5. The optical characteristics of bivacancies ($v_a v_c$), the number of which drastically increases in an MgO crystal exposed to a plastic stress, have been revealed using VUV-radiation of 4–35 eV at 9 K. The luminescence bands peaked at 2.9 and 5.2 eV have been attributed to the recombination of a hole/electron with its counterpart previously trapped at a $v_a v_c$:



So, the long-known observation that the 2.9 eV emission is strongly enhanced in a plastically deformed, prepared by additive coloration, or SHI-

irradiated MgO sample, can be explained by a significant deformation of a crystalline lattice, causing the increased number of $v_a v_c$.

6. The excitation processes of cubic and axial tetragonal Cr^{3+} centers ($[\text{Cr}]^+$ and $[\text{Cr}-\text{O}-v_c]$) have been investigated for the first time for virgin or X-ray irradiated $\text{MgO}:\text{Cr}^{3+}$ (100 and 850 ppm) crystals using synchrotron radiation of 4–32 eV at 9 K. The excitation spectra for R- and N-lines of Cr^{3+} emission have been constructed on the basis of a series of emission spectra recorded by a CCD detector. The excitation spectra for cubic and axial tetragonal Cr^{3+} centers in a virgin sample are rather different from those measured for a crystal previously X-irradiated at RT. In an irradiated sample, the emission efficiency decreases by a factor of 2 at the direct intracenter excitation (6–6.5 eV), while at $h\nu > 20$ eV it is about 3 and 5 times higher for cubic and tetragonal centers, respectively. It was shown earlier by the EPR method that single cubic Cr^{3+} centers serve as electron traps (i.e. Cr^{2+} centers) stable up to ~ 700 K. The recombination of h released from trapped-hole centers with Cr^{2+} results in the emission of cubic Cr^{3+} centers, the intensity of which increases under conditions of $e-h$ multiplication.

A broad emission band peaking around 1.6 eV is connected with a rhombic pair chromium center $[\text{Cr}-v_c-\text{Cr}]^0$ that could serve as a hole trap. In X- (50 keV) or electron irradiated (5–10 keV) $\text{MgO}:\text{Cr}^{3+}$ (850 ppm) crystals, holes become localized at oxygen ions (atomic mass of 16) near heavy ($52 + 52 = 104$) rhombic pair chromium clusters $[\text{Cr}-v_c-\text{Cr}]^0$. A subsequent recombination of high-energy electrons with such holes results in an energy release sufficient for the formation of anharmonic ultrasonic vibrations causing a rearrangement of many host ions. The annealing of these 3D defects occurs at significantly higher temperatures than that of close Frenkel pairs.

7. The irradiation of highly pure or doped (Be^{2+} , Ca^{2+} , Al^{3+} , Cr^{3+} , Fe^{3+} , OH^-) MgO single crystals with SHI (~ 2 GeV, ^{198}Au , ^{238}U , range about 50 μm) leads to the formation of cylindrical ion tracks, where more than 99% of the absorbed energy is spent on ionization losses ($LET > 20$ keV/nm). MgO crystals sustain SHI-irradiation with a fluence of up to 10^{13} ions/cm², while a cracking of complex metal oxides with heavy rare-earth cations (e.g., Gd_2SiO_5) occurs already at considerably lower fluences. The nonimpact creation of F and F^+ centers, single anion vacancies and oxygen interstitials as well as bivacancies ($v_a v_c$), F_2 centers and more complex defects has been detected at a periphery of ion tracks using absorption and luminescence methods. The number of radiation-induced defects significantly exceeds the number of as-grown imperfections.

The annealing of complex 3D defects induced by SHI-irradiation in MgO single crystals doped with heavy trivalent ions occurs at higher temperatures than that for elementary FD formed at a periphery of ion tracks. 3D defects serve as stoppers for dislocations, thus, facilitating the appearance of microcracks. Among our doped and non-doped MgO crystals, highly pure

stoichiometric single crystals demonstrate the highest resistance against irradiation with SHIs. A quantitative study of the influence of certain impurity ions (e.g., pair Cr^{3+} - Cr^{3+} and Ni^{2+} - Ni^{2+} centers) on the efficiency of radiation damage of MgO by SHIs still lies ahead. Particular emphasis should be laid on luminescent divalent nickel ions, a large concentration of which can be introduced into MgO crystals.

KOKKUVÕTE

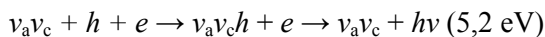
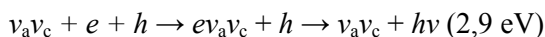
Struktuuridefektide tekkeprotsessid puhastes ja dopeeritud MgO ja NaCl monokristallides madala ja ülikõrge elektronergastuste tiheduse tingimustes

Peamisteks uurimisobjektideks olid kõrge puhtusega ja dopeeritud NaCl ja MgO monokristallid, mis olid kasvatatud Tartu Ülikooli Füüsika Instituudis. Nendel kristallidel on sama tahkkeskendatud kuupvõre ja lähedased keelutsooni laiused (vastavalt ~8,8 ja 7,8 eV NaCl-s ja MgO-s), kuid väga erinevad sulamistemperatuurid (1074 ja ~3200 K) ja erinev aukude ja eksitonide käitumine. Frenkeli paari moodustumisenergia ületab keelutsooni laiuse nii NaCl (kui $T < 120$ K), kui ka MgO kristallis: $E_{FD} > E_g$. Nende materjalide võrdlev kompleksne uurimine hõlmas kiirituskindlust ja Frenkeli defektide ja nende komplekside elementaarseid tekkemehhanisme 6–40 eV footonitega, röntgenkiirgusega (~50 keV), elektronidega (4–20 keV) ja raskete ionidega (^{198}Au , ^{238}U , ~GeV, MgO juhul) kiiritamisel. Objektide uurimiseks kasutati optilise ja termooaktivatsioonspektroskoopia meetodeid laias temperatuurivahemikus (6–875 K). Peamised tulemused nanosuurusel kiiritusdefektide tekkemehhanismide ja kiirgusliku kahjustuse efektiivsuse mõjutamisvõimaluste osas on järgmised:

1. Kasutades kõrge tundlikkusega luminesentsmeetodit ja 7–40 eV VUV kiirgust, on mõõdetud pikaealiste ($\tau > 1$ s) anioonsete Frenkeli defektipaaride (F-H paarid defektide vahekaugusega mitu võrekonstanti) tekkespekter 12 K juures kõrge puhtusega NaCl monokristallis, mis madalatel temperatuuridel näitab üsna kõrget kiirituskindlust ($E_{FD} > E_g$). On leidnud kinnitust, et pikaealiste FD tekke efektiivsus (η_{FH}) iselõksustunud eksitonide (STE) lagunemisel või relakseerunud elektronide rekombinatsioonil iselõksustunud aukudega on väga madal, samal ajal kui järsk η_{FH} tõus ilmneb 12–16 eV ergastamisel, mille korral ergastav footon ei ole veel suuteline tekitama kordistumisprotsessi, vaid tekitab kuumat $e-h$ paari, ja sellise paari rekombineerumisel vabanev energia ületab E_{FD} . F-H paaride tekke efektiivsus kahekordistub, kui ergastav footon energiaga 28–32 eV moodustab juba kaks kuumat $e-h$ paari, kuid ~33–34 eV juures katiooneksitoni fototekkel toimub järsk η_{FH} langus. H-tsentrite hüppedifusioon algab $T > 30$ K ja sellega kaasneb nende EPR-signaali langus ja TSL piik ~35 K juures, mis koosneb peamiselt tripletsete iselõksustatud eksitonide kiirgusest 3,4 eV. Meie arvates see kiirgus tuleneb lähedaste F- ja H-tsentrite rekombinatsioonist ergastatud STE seisundi kaudu („STE kiirguslik kooslus”).
2. NaCl kuumutamine üle 120 K viib kristallvõre anharmoonilise paisumiseni, ja E_{FD} väärtus väheneb ($E_{FD} < E_g$), soodustades FD tekkimist kõrgetel temperatuuridel. Samal ajal, kuumade laengukandjate panust F-H paaride ja nende komplekside moodustumisse kristalli mahus näidati optilise neeldumise meetodiga kõrge puhtusega NaCl ja KCl kristallides, mis olid kiiritatud laseriga toatemperatuuril kahefootonilise neeldumise režiimis (kristallid olid

1–3 mm sügavuselt ühtlaselt värvunud). Kiiritamine KrF laseriga ($2 \times 4,99 \text{ eV} = 9,98 \text{ eV}$) põhjustab peamiselt külmade (relakseerunud) $e-h$ paaride tekkimist, ArF laser ($2 \times 6,42 \text{ eV} = 12,84 \text{ eV}$) aga tekitab kuumi ja ruumiliselt eraldatud e ja h . Mobiilsete valentsaukude olemasolu suurendab järsult termiliselt stabiilsete defektikomplekside – F_2 tsentrite ja X_3^- kolmikhalogeentsentrite – tekkimise efektiivsust kristalli ruumalas.

3. Tahkise Franck-Hertz efekti analoogi (TFHEA) – lisandiooni otsese ergastamise kuumade juhtivuselektronidega, mille energiast veel ei piisa sekundaarsete eksitonide või $e-h$ paaride tekkimiseks – ilmumine on näidatud dopeeritud NaCl ja MgO kristallide foto- ja katoodluminesentsis. Leelishalogeniidides (näiteks, NaCl:TI^+) TFHEA-d võib vaadelda kui luminesentskaitset FD mittepõrke tekkemehhanismi vastu, kuna kuum juhtivuselektron kaotab osa oma energiast TFHEA kaudu (st. kiirgusliku kanali kaudu), niiviisi vähendades FD tekke efektiivsust järgnevas „jahtunud“ e ja h rekombinatsioonis. Kuid MgO:Cr^{3+} -s on TFHEA mõju kiirituskindlusele märgatavalt väiksem, sest mittepõrke- $E_{\text{FD}} \approx 30 \text{ eV}$, nii et on raske luua tingimusi piisavalt kuumade $e-h$ paaride tekkeks $e-h$ kordistumisprotsessiga konkureerimise tõttu.
4. Rida lisanditega seotud madalaid auklõkse – eriti Ca^{2+} and Be^{2+} ioonid – on tuvastatud MgO kristallis, kus ei toimu ei elektronide, aukude, ega suure raadiusega eksitonide iselõksustamist. Need lisandioonid on isovalentsed Mg^{2+} katioonidega, ja augud lõksustuvad naaber-hapniku ioonil peamiselt lokaalse võredeformatsiooni tõttu. Selline auk-tsenter omab positiivset elektrilaengut regulaarse võre suhtes ($[\text{hCa}]^+$, $[\text{hBe}]^+$) ja suurt ristlõiget kuumade juhtivuselektronidega rekombineerumiseks, seega tekitab soodsaid tingimusi FD mittepõrkeliseks tekkeks. See kehtib isegi nende tsentrite ioniseerimistemperatuurist kõrgematel temperatuuridel, sest augud võivad ikkagi lõksustuda lühiajaks. See tulemus näitab MgO teatud lisanditest puhastamise tähtsust kiirituskindluse suurendamiseks.
5. Bivakantside ($v_a v_c$) arv suureneb järsult MgO kristallides plastilise deformatsiooni mõjul; nende defektide optilised omadused on välja selgitatud, kasutades VUV kiirgust 4–35 eV 9 K juures. Kiirgusribad maksimumidega 2,9 ja 5,2 eV juures omistati augu/elektroni rekombinatsioonile bivakantsil lõksustatud vastas-laengukandjaga:



Seega, ammune tähelepanek, et kiirgus 2,9 eV tugevneb plastiliselt deformeeritud, additiivselt värvitud või raskete ionidega kiiritatud MgO kristallides, võib olla seletatud kristallivõre märgatava deformatsiooniga, mis põhjustab $v_a v_c$ arvu kasvu.

6. Kuubiliste ja aksiaalsete tetragonaalsete Cr^{3+} tsentrite ($[\text{Cr}]^+$ ja $[\text{Cr-O-}v_c^-]$) ergastusprotsessid olid esimest korda uuritud kiiritamata või röntgenkiirgusega kiiritatud $\text{MgO}:\text{Cr}^{3+}$ (100 ja 850 ppm) kristallides, kasutades sünkrotronkiirgust 4–32 eV temperatuuril 9 K. Cr^{3+} R- ja N-kiirgusjoonte ergastusspektrid olid konstrueeritud CCD-detektoriga registreeritud kiirgusspektrite seeria baasil. Kuubiliste ja tetragonaalsete Cr^{3+} tsentrite ergastusspekterid kiiritamata ja toatemperatuuril röntgeniseeritud proovides on küllaltki erinevad. Kiiritatud proovis luminesentsi efektiivsus väheneb otsesel tsentrisisesel ergastusel (6–6,5 eV) 2 korda, samal ajal kui ergastuse $h\nu > 20$ eV efektiivsus on, vastavalt, kuubilistel ja tetragonaalsetel tsentritel, 3 ja 5 korda kõrgem. EPR meetodiga oli varem näidatud, et üksikud kuubilised Cr^{3+} tsentrid käituvad elektronide löksudena (moodustades Cr^{2+}), mis on stabiilsed kuni ~ 700 K. Auktsentritelt vabanenud aukude rekombinatsioon Cr^{2+} tsentritega põhjustab kuubiliste Cr^{3+} tsentrite kiirgust, mille intensiivsus kasvab $e-h$ kordistumise tingimustes.

Lai kiirgusriba maksimumiga $\sim 1,6$ eV on seotud rombiline sümmeetriaga paariskroomtsentriga $[\text{Cr-}v_c\text{-Cr}]^0$, mis võib toimida augu löksuna. Röntgenkiirgusega (50 keV) või elektronidega (5–10 keV) kiiritatud $\text{MgO}:\text{Cr}^{3+}$ (850 ppm) kristallides augud lokaliseeruvad hapniku ioonidel (aatommass 16) raske ($52 + 52 = 104$) rombiline paaritsentri $[\text{Cr-}v_c\text{-Cr}]^0$ kõrval. Kõrgenergeetilise elektronide ja niisuguste aukude järgnevas rekombinatsioonis eraldub piisavalt energiat anharmooniliste ultraheli võngete formeerumiseks, mis põhjustavad paljude ümbritsevate ioonide ümberpaiknemist. Nende kolmemõõtmeliste defektide lõõmutus toimub oluliselt kõrgemal temperatuuril, kui lähedaste Frenkeli paaride juhul.

7. Kõrge puhtusega või dopeeritud (Be^{2+} , Ca^{2+} , Al^{3+} , Cr^{3+} , Fe^{3+} , OH^-) MgO monokristallide ($E_{\text{FD}} > E_g$) kiiritamine raskete ioonidega (~ 2 GeV, ^{198}Au , ^{238}U , sügavus ligikaudu 50 μm) viib silindriliste iointrekkide tekkimiseni, kus üle 99% neeldunud energiast on kulunud ionisatsioonikadudele (elektronergastuste teke, kui $\text{LET} > 20$ keV/nm). MgO kristallid taluvad ionivoogusid kuni 10^{13} ioone/ cm^2 , samal ajal kui raskeid haruldasi leelismuld katioone sisaldavate komplekssete metalloksiidide (nt. Gd_2SiO_5) pragunemine toimub juba märgatavalt madalamatel voogudel. Nii F ja F^+ tsentrid, üksikud anioonvakantsid, hapniku interstitsiaalid, kui ka bivakantsid ($v_a v_c$), F_2 tsentrid ja keerulisemad defektid olid detekteeritud iointrekkide välispiirkonnas neeldumis- ja luminesentsmeetoditega. Kiiritusdefektide arv ületab oluliselt kasvudefektide arvu. Dopeeritud ja dopeerimata MgO kristallidest kõige kõrgemat kiirituskindlust raskete ioonide vastu omab kõrge puhtusega stöhhiomeetriline monokristall. Kindlate lisandioonide (s. h paarsete $\text{Cr}^{3+}\text{-Cr}^{3+}$ ja $\text{Ni}^{2+}\text{-Ni}^{2+}$ tsentrite) mõju uurimine raskete ioonide põhjustatud kiirguskahjustusele seisab ees. Erilist tähelepanu peaks osutama luminesseeruvatele divalentsetele nikliioonidele, mis võivad olla MgO kristallidesse sisse viidud suurtes kontsentratsioonides.

AKNOWLEDGEMENTS

I would like to thank my supervisors Prof. Aleksandr Lushchik and Dr. Evgeni Vassil'chenko for guiding me during the years that were needed to complete this thesis. I appreciate their patience with me.

I am also grateful to Prof. Cheslav Lushchik for productive discussions and help with writing the thesis, to Dr. Aarne Maaros for preparation of the crystals which were the basis for this thesis, to Drs. Aleksei Kotlov, Vitali Nagirnyj, and Tiit Kärner for their help in conducting experiments and providing answers to related questions, and to Prof. Kurt Schwartz for providing irradiation of objects with swift heavy ions.

I am thankful to all my colleagues in the Laboratory of Ionic Crystals for providing a friendly and fruitful working atmosphere.

The study has been supported by the Estonian Science Foundation (grants No. 6652, 7825), Estonian Ministry of Education and Research (targeted project SF0180037s07), and Graduate School on Functional Materials and Technologies (GSFMT) of the University of Tartu.

REFERENCES

- [1] N. Itoh and A. M. Stoneham, *Material Modification by Electronic Excitation*, Univ. Press, Cambridge (2000)
- [2] Ch. B. Lushchik; A. Ch. Lushchik, *Decay of Electronic Excitations with Defect Formation in Solids*. Nauka, Moscow (1989). (Ч.Б.Лущик, А.Ч.Лущик, “Распад электронных возбуждений с образованием дефектов в твёрдых телах”, М. Наука (1989))
- [3] K. S. Song and R.T. Williams, *Self-Trapped Excitons*, Second Ed., Heidelberg, Springer, Berlin (1996)
- [4] Ch. B. Lushchik, I. K. Vitol, M. A. Elango, *Uspekhi Fizicheskikh Nauk* **122**(2), 223–251 (1977)
- [5] Y. Chen, M. M. Abraham, *J. Phys. Chem. Solids* **51**, 747–764 (1990)
- [6] B. Henderson and J. E. Wertz, *Defects in the Alkaline Earth Oxides*, Taylor & Francis Ltd, London (1977)
- [7] A. J. Sievers and S. Takedo, *Phys. Rev. Lett.* **61**, 970 (1988)
- [8] M. Haas, V. Hizhnyakov, A. Shelkan, M. Klopov, and A. J. Sievers, *Phys. Rev. B* **84**, 144303 (2011)
- [9] V. E. Zakharov and E. A. Kuznetsov, *Phys. Usp.* **55**(6), (2012) [*Uspekhi Fiz. Nauk* **55**, 569 (2012)]
- [10] F. Stöber, *Z. Kristallogr.* **61**, 299 (1925)
- [11] M. M. Abraham, C. T. Butler, and Y. Chen, *J. Chem. Phys* **55** (8), 3752–3756 (1971)
- [12] C. T. Butler, B. J. Sturm, and R. B. Quincy Jr., *J. Cryst. Growth* **8**, 197–204 (1971)
- [13] A. Maaros, *Akademiya Nauk Estonskoi SSR. Trudy Instituta Fiziki* **53**, 49 (1982)
- [14] G. Zimmerer, *Rad. Meas.*, **42**, 859–864 (2007)
- [15] J. V. Sharp, D. Rumsby, *Radiat. Eff.* **17**(1), 65–68 (1973)
- [16] A. Ch. Lushchik, Ch. B. Lushchik, *Bulletin of the Russian Academy of Sciences. Physics*, **56** (2), 201–206 (1992) (А.Ч.Лущик, Ч.Б.Лущик, *Изв. РАН. Сер. физ.*, **56**, 88–95 (1992))
- [17] H. Guo, M. Zhang, J. Han, H. Zhang, and N. Song, *Physica B* **404**, 2262 (2012).
- [18] E. Balanzat, S. Bouffard, A. Cassimi, E. Dooryhee, J. P. Grandin, J. L. Doualan, J. Margerie, *Nucl. Instr. And Meth B* **91**, 134 (1994)
- [19] K. Schwartz, C. Trautmann, A. S. El-Said, R. Neumann, M. Toulemonde, W. Knolle, *Phys. Rev. B* **70**, 184104 (2004)
- [20] K. Schwartz, A. E. Volkov, K.-O. Voss, M. V. Sorokin, C. Trautmann, R. Neumann, *Nucl. Instr. And Meth B* **245**, 204–209 (2006)
- [21] R. L. Fleischer, P. B. Price, and R. M. Walker, *J of App. Phys* **36**, 11, 3645–3652 (1965)
- [22] D. A. Young, *Europhys. Lett.* **59**(4), 540–545 (2002)
- [23] D. Schoemaker, *Phys. Rev. B* **7**, 78 (1973)
- [24] A. Ch. Lushchik, J. V. Kolk, N. E. Lushchik, A. G. Frorip, *Akademiya Nauk Estonskoi SSR. Trudy Instituta Fiziki* **58**, 25–46 (1986)
- [25] M. N. Kabler, D. A. Patterson, *Phys. Rev. Lett.* **19**, 652 (1967)
- [26] J. H. Schulman, W. D. Compton, *Color centers in solids*, p. 345, Pergamon Press. N. Y. (1963)

- [27] Ch. B. Lushchik, E. A. Vasil'chenko, N. E. Lushchik, L. A. Pung, *Akademiya Nauk Estonskoi SSR. Trudy Instituta Fiziki* **39**, 3–46 (1972)
- [28] W. Kanzig, T. Woodruff, *J. Phys. Chem. Solids* **9**, 7092 (1958)
- [29] E.A. Kotomin, A.I. Popov, *Radiation Effects in Solids*, Edited by Kurt E. Sickafus, Eugen A. Kotomin and Blas P. Uberuaga, **235**, 153–192, Springer, Amsterdam (2007)
- [30] Ch. B. Lushchik, G. G. Liidya, M. A. Elango, *Sov. Phys. Solid. State*, **6**, 1789 (1965)
- [31] Ch. B. Lushchik, J. V. Kolk, A. Ch. Lushchik, N. E. Lushchik, M. Taiiroov, E. A. Vasilchenko, *Phys. Stat. Solidi B* **114**, 103 (1982)
- [32] E. Feldbach, M. Kirm, A. Ch. Lushchik, Ch. B. Lushchik and I. Martinson, *J. Phys.: Condens. Matter* **12**, 1991–2005 (2000)
- [33] F.-J. Himpsel, W. Steinmann, *Phys. Rev. B* **17**, 2537 (1978)
- [34] Yu. M. Aleksandrov, Ch. B. Lushchik, V. N. Makhov, T. I. Syreishchikova, and M. N. Yakimenko, *Sov. Phys. Solid State* **24**, 968 (1982)
- [35] E. Feldbach, M. Kamada, M. Kirm, A. Lushchik, Ch. Lushchik, I. Martinson, *Phys. Rev. B* **56**, 13908–13915 (1997)
- [36] A. Ch. Lushchik, M. Kamada, M. Kirm, Ch. B. Lushchik, I. Martinson, *Radiat. Meas.* **29**, 229–334 (1998).
- [37] A. Lushchik, Ch. Lushchik, M. Kirm, V. Nagirnyi, F. Savikhin, E. Vasil'chenko, *Nucl. Instrum. Methods B* **250**, 330–336 (2006)
- [38] Yu. M. Aleksandrov, A. N. Vasil'ev, V. N. Kolobanov, Ch. B. Lushchik, A. A. Maaros, V. N. Makhov, V. V. Mikhailin, T. I. Syreishchikova, M. N. Yakimenko, *Trudy Instituta Fiziki* **53**, 31, (1982)
- [39] A. N. Vasil'ev, V. N. Kolobanov, I. L. Kuusmann, Ch. B. Lushchik, V. V. Mikhailin, *Sov. Phys. Solid State* **27**, 1616 (1985)]
- [40] Z. A. Rachko, J. A. Valbis, *Phys. Stat. Solidi B* **93**, 161–166 (1979)
- [41] P. V. Sushko, A. L. Shluger, C. R. Catlow, *Surf. Sci.* **450**, 153 (2000)
- [42] B. Henderson, J. E. Wertz, *Adv. Phys.* **17**, 749–855 (1968).
- [43] O. F. Schirmer, *J. Phys.: Condens. Matter* **18**, R667 (2006)
- [44] W. C. Mackrodt, R. F. Stewart, *J. Phys. C: Solid State Phys.* **12**, 5015 (1979)
- [45] J. E. Wertz, J. W. Orton, and P. Auzins, *Discussions Faraday Soc.* **31**, 140–150 (1961)
- [46] Y. Chen, J.L. Kolopus, and W.A. Sibley, *Phys. Rev.* **186**, 865 (1969)
- [47] Y. Chen, J.L. Kolopus, and W.A. Sibley, *J. Lumin* **1** (2), 633 (1970)
- [48] M. Nakagawa, *J. Phys. Soc. Japan* **24**, 1027 (1968)
- [49] R. Gonzales, Y. Chen, R. M. Sebek, G. P. Williams Jr., R. T. Williams, and W. Gellermann, *Phys. Rev. B* **43**, 5228 (1991)
- [50] D. O. O'Connell, B. Henderson, and J. M. Bolton, *Sol. State Commun.* **38**, 283 (1981)
- [51] J. D. Bolton, B. Henderson, D. O. O'Connell, *Sol. State Commun.* **38**, 287 (1981)
- [52] Y. Chen, M. M. Abraham, T. J. Turner, and C.M. Nelson, *Phil. Mag.* **32**, 99 (1975)
- [53] B. Henderson, *J. Phys. C* **9** (20), 1579–1584 (1976)
- [54] L. A. Kappers, F. Dravnieks, J. E. Wertz, *J. Phys. C*, **7** (7), 1387–1399 (1974)
- [55] M. M. Abraham, Y. Chen, L. A. Beatner, R. W. Reynolds, *Phys. Rev. Lett.* **37** (13), 849–852 (1976)
- [56] M. M. Abraham, Y. Chen, J. L. Kolopus, H. T. Tohver, *Phys. Rev. B* **5** (12), 4945–4951 (1972)

- [57] O. F. Schirmer, *Z. Physik. B* **24** (3), 235–244 (1976)
- [58] L. A. Kappers, F. Dravnieks, J. E. Wertz, *Solid St. Commun.* **10** (12), 1265–1269 (1972)
- [59] Y. Chen, H. T. Tohver, J. Narayan, M. M. Abraham, *Phys. Rev. B* **16** (12), 5535–5542 (1977)
- [60] N. A. Mironova, U. A. Ulmanis, *Radiation defects and ions of Fe-group metals in oxides*, 67, Zinatne, Riga (1988)
- [61] L. E. Halliburton, L.A. Kappers, *Solid State Commun.* **26**, 111 (1978)
- [62] T. Brudevoll, E. A. Kotomin, and N. E. Christensen, *Phys. Rev. B* **53**, 7731 (1996)
- [63] R. A. Evarestov, P. W. M. Jacobs, and A. V. Leko, *Phys. Rev. B* **54**, 8969 (1996)
- [64] E. A. Kotomin and A. I. Popov, *Nucl. Instr. and Meth. B* **141**, 1 (1998)
- [65] T. N. Kärner, A. F. Malysheva, A. A. Maaros, V. V. Mürk, *Sov. Phys. Solid State (USA)* **22**, 1178–1183 (1980)
- [66] J. M. Luthra, A. Sathyamoorthy, and N. M. Gupta, *J. Lumin.* **15**, 395 (1977)
- [67] M. A. Monge, A. I. Popov, C. Ballesteros, R. González, Y. Chen, E. A. Kotomin, *Phys. Rev. B* **62** (14), 9299–9304 (2000)
- [68] A. Ch. Lushchik, Ch. B. Lushchik, N. E. Lushchik, A. G. Frorip, O. Nikiforova, *Phys. Status Solidi B* **168**, 413 (1991)]
- [69] F. Seitz, *Phys. Rev.* **89**, 1299 (1953)
- [70] S. A. Dolgov, V. Isakhanyan, T. N. Kärner, P. Liblik, A. A. Maaros, S. Nako-nechnyj, *Rad. Meas.* **38**, 699–702 (2004)
- [71] E. Feldbach, Ch. B. Lushchik, I. L. Kuusmann, *Letters in JETF* **39**, 54–56 (1984)
- [72] E. Feldbach, I. L. Kuusmann, G. Zimmerer, *J. Lumin.* **24/25**, 433–436 (1981)
- [73] M. Kirm, A. Ch. Lushchik, Ch. B. Lushchik, and E. A. Vasil’chenko, Relaxation of hot photocarriers created by VUV photons in wide-gap crystals, *Physics and Chemistry of Luminescent Material*, eds. C.W. Struck, K.C. Mishra and B. DiBartolo, vol. PV **98**–24, 267–276, The Electrochemical Society Proceedings Series, Pennington, NJ (1999)
- [74] M. Kirm, E. Feldbach, T. N. Kärner, A. Ch. Lushchik, Ch. B. Lushchik, A. A. Maaros, V. Nagirnyi, and I. Martinson, *Nucl. Instrum Methods B.* **141**, 431–435 (1998)
- [75] K. A. Kalder, T. N. Kärner, Ch. B. Lushchik, A. F. Malysheva, R. V. Milenina, *Zh. Prikl. Spektrosk.* **25**, 639–644 (1976)
- [76] A. Ch. Lushchik, Ch. B. Lushchik, M. Kirm, V. Nagirnyi, F. Savikhin, E. A. Vasil’chenko, *Nucl. Instr. Meth. B* **250**, 330–336 (2006)
- [77] A. Boyrivent, E. Duval, *J. Phys. C: Solid State Phys.* **11**, 439–448 (1978)]
- [78] G. F. Imbusch, A. L. Schawlow, A. D. May, and S. Sugano, *Phys. Rev.* **140**, A830 (1965)
- [79] M.O. Henry, J.P. Larkin, and G.F. Imbusch, *Phys. Rev. B* **13**, 5, 1893–1902 (1976)
- [80] R. C. Whited, W. C. Walker, *Phys. Rev. Lett.* **22**, 1428 (1969)
- [81] S. Kück, E. Heumann, T. N. Kärner, and A. A. Maaros, *Optics Letters* **24**, 966 (1999)
- [82] W. M. Yen, L. R. Elias, and D. L. Huber, *Phys. Rev. Lett.* **24**, 1011 (1970)
- [83] T. N. Kärner, A. A. Maaros, A. F. Malysheva, B. T. Tazhigulov, *Fizika Tverdogo Tela* **28**, 2563–2565 (1986)

PUBLICATIONS

CURRICULUM VITAE

Name: Jevgeni Shablonin
Date of birth: 23.08.1984
Citizenship: Estonian
Telephone: +372 5381 4585, +372 5825 8600
E-mail: jevgis@ut.ee

Education:
2008–present University of Tartu, PhD studies
2006–2008 University of Tartu, 2008, M.Sc
2003–2006 University of Tartu, 2006, B.Sc
1991–2003 Karjamaa Gymnasium, Tallinn

Professional employment:
2009–present University of Tartu, Institute of Physics, engineer

Language skills:
Russian mother tongue
Estonian good in speaking and writing
English good in speaking and writing

Main field of research:
Spectroscopy and radiation physics of ionic crystals

ELULOOKIRJELDUS

Nimi: Jevgeni Šablonin
Sünniaeg: 23.08.1984
Kodakondsus: Eesti
Telephone: 5381 4585, 5825 8600
E-mail: jevgis@ut.ee

Haridus:
2008–k.a. Tartu Ülikool, doktoriõpe
2006–2008 Tartu Ülikool, 2008, M.Sc
2003–2006 Tartu Ülikool, 2006, B.Sc
1991–2003 Karjamaa Gümnaasium, Tallinn

Teenistuskäik:
2009–k.a. Tartu Ülikool, Füüsikainstituut, insener

Keelteoskus:
Russian emakeel
Estonian hea kirjas ja kõnes
English hea kirjas ja kõnes

Peamine uurimisvaldkond:
Ioonkristallide spektroskoopia ja kiiritusfüüsika

DISSERTATIONES PHYSICAE UNIVERSITATIS TARTUENSIS

1. **Andrus Ausmees.** XUV-induced electron emission and electron-phonon interaction in alkali halides. Tartu, 1991.
2. **Heiki Sõnajalg.** Shaping and recalling of light pulses by optical elements based on spectral hole burning. Tartu, 1991.
3. **Sergei Savihhin.** Ultrafast dynamics of F-centers and bound excitons from picosecond spectroscopy data. Tartu, 1991.
4. **Ergo Nõmmiste.** Leelishalogeniidide röntgenelektronemissioon kiiritamisel footonitega energiaga 70–140 eV. Tartu, 1991.
5. **Margus Rätsep.** Spectral gratings and their relaxation in some low-temperature impurity-doped glasses and crystals. Tartu, 1991.
6. **Tõnu Pullerits.** Primary energy transfer in photosynthesis. Model calculations. Tartu, 1991.
7. **Olev Saks.** Attoampri diapsoonis voolude mõõtmise füüsikalised alused. Tartu, 1991.
8. **Andres Virro.** AlGaAsSb/GaSb heterostructure injection lasers. Tartu, 1991.
9. **Hans Korge.** Investigation of negative point discharge in pure nitrogen at atmospheric pressure. Tartu, 1992.
10. **Jüri Maksimov.** Nonlinear generation of laser VUV radiation for high-resolution spectroscopy. Tartu, 1992.
11. **Mark Aizengendler.** Photostimulated transformation of aggregate defects and spectral hole burning in a neutron-irradiated sapphire. Tartu, 1992.
12. **Hele Siimon.** Atomic layer molecular beam epitaxy of A^2B^6 compounds described on the basis of kinetic equations model. Tartu, 1992.
13. **Tõnu Reinot.** The kinetics of polariton luminescence, energy transfer and relaxation in anthracene. Tartu, 1992.
14. **Toomas Rõõm.** Paramagnetic H^{2-} and F^+ centers in CaO crystals: spectra, relaxation and recombination luminescence. Tallinn, 1993.
15. **Erko Jalviste.** Laser spectroscopy of some jet-cooled organic molecules. Tartu, 1993.
16. **Alvo Aabloo.** Studies of crystalline celluloses using potential energy calculations. Tartu, 1994.
17. **Peeter Paris.** Initiation of corona pulses. Tartu, 1994.
18. **Павел Рубин.** Локальные дефектные состояния в CuO_2 плоскостях высокотемпературных сверхпроводников. Тарту, 1994.
19. **Olavi Ollikainen.** Applications of persistent spectral hole burning in ultrafast optical neural networks, time-resolved spectroscopy and holographic interferometry. Tartu, 1996.
20. **Ülo Mets.** Methodological aspects of fluorescence correlation spectroscopy. Tartu, 1996.
21. **Mikhail Danilkin.** Interaction of intrinsic and impurity defects in CaS:Eu luminophors. Tartu, 1997.

22. **Ирина Кудрявцева.** Создание и стабилизация дефектов в кристаллах KBr, KCl, RbCl при облучении ВУФ-радиацией. Tartu, 1997.
23. **Andres Osvet.** Photochromic properties of radiation-induced defects in diamond. Tartu, 1998.
24. **Jüri Örd.** Classical and quantum aspects of geodesic multiplication. Tartu, 1998.
25. **Priit Sarv.** High resolution solid-state NMR studies of zeolites. Tartu, 1998.
26. **Сергей Долгов.** Электронные возбуждения и дефектообразование в некоторых оксидах металлов. Tartu, 1998.
27. **Кауро Кукли.** Atomic layer deposition of artificially structured dielectric materials. Tartu, 1999.
28. **Ivo Heinmaa.** Nuclear resonance studies of local structure in $\text{RBa}_2\text{Cu}_3\text{O}_{6+x}$ compounds. Tartu, 1999.
29. **Aleksander Shelkan.** Hole states in CuO_2 planes of high temperature superconducting materials. Tartu, 1999.
30. **Dmitri Nevedrov.** Nonlinear effects in quantum lattices. Tartu, 1999.
31. **Rein Ruus.** Collapse of 3d (4f) orbitals in 2p (3d) excited configurations and its effect on the x-ray and electron spectra. Tartu, 1999.
32. **Valter Zazubovich.** Local relaxation in incommensurate and glassy solids studied by Spectral Hole Burning. Tartu, 1999.
33. **Indrek Reimand.** Picosecond dynamics of optical excitations in GaAs and other excitonic systems. Tartu, 2000.
34. **Vladimir Babin.** Spectroscopy of exciton states in some halide macro- and nanocrystals. Tartu, 2001.
35. **Toomas Plank.** Positive corona at combined DC and AC voltage. Tartu, 2001.
36. **Kristjan Leiger.** Pressure-induced effects in inhomogeneous spectra of doped solids. Tartu, 2002.
37. **Helle Kaasik.** Nonperturbative theory of multiphonon vibrational relaxation and nonradiative transitions. Tartu, 2002.
38. **Tõnu Laas.** Propagation of waves in curved spacetimes. Tartu, 2002.
39. **Rünno Lõhmus.** Application of novel hybrid methods in SPM studies of nanostructural materials. Tartu, 2002.
40. **Kaido Reivelt.** Optical implementation of propagation-invariant pulsed free-space wave fields. Tartu, 2003.
41. **Heiki Kasemägi.** The effect of nanoparticle additives on lithium-ion mobility in a polymer electrolyte. Tartu, 2003.
42. **Villu Repän.** Low current mode of negative corona. Tartu, 2004.
43. **Алексей Котлов.** Оксианионные диэлектрические кристаллы: зонная структура и электронные возбуждения. Tartu, 2004.
44. **Jaak Talts.** Continuous non-invasive blood pressure measurement: comparative and methodological studies of the differential servo-oscillometric method. Tartu, 2004.
45. **Margus Saal.** Studies of pre-big bang and braneworld cosmology. Tartu, 2004.

46. **Eduard Gerškevičš.** Dose to bone marrow and leukaemia risk in external beam radiotherapy of prostate cancer. Tartu, 2005.
47. **Sergey Shchemelyov.** Sum-frequency generation and multiphoton ionization in xenon under excitation by conical laser beams. Tartu, 2006.
48. **Valter Kiisk.** Optical investigation of metal-oxide thin films. Tartu, 2006.
49. **Jaan Aarik.** Atomic layer deposition of titanium, zirconium and hafnium dioxides: growth mechanisms and properties of thin films. Tartu, 2007.
50. **Astrid Rekker.** Colored-noise-controlled anomalous transport and phase transitions in complex systems. Tartu, 2007.
51. **Andres Punning.** Electromechanical characterization of ionic polymer-metal composite sensing actuators. Tartu, 2007.
52. **Indrek Jõgi.** Conduction mechanisms in thin atomic layer deposited films containing TiO₂. Tartu, 2007.
53. **Aleksei Krasnikov.** Luminescence and defects creation processes in lead tungstate crystals. Tartu, 2007.
54. **Küllike Rägo.** Superconducting properties of MgB₂ in a scenario with intra- and interband pairing channels. Tartu, 2008.
55. **Els Heinsalu.** Normal and anomalously slow diffusion under external fields. Tartu, 2008.
56. **Kuno Kooser.** Soft x-ray induced radiative and nonradiative core-hole decay processes in thin films and solids. Tartu, 2008.
57. **Vadim Boltrushko.** Theory of vibronic transitions with strong nonlinear vibronic interaction in solids. Tartu, 2008.
58. **Andi Hektor.** Neutrino Physics beyond the Standard Model. Tartu, 2008.
59. **Raavo Josepson.** Photoinduced field-assisted electron emission into gases. Tartu, 2008.
60. **Martti Pärs.** Study of spontaneous and photoinduced processes in molecular solids using high-resolution optical spectroscopy. Tartu, 2008.
61. **Kristjan Kannike.** Implications of neutrino masses. Tartu, 2008.
62. **Vigen Issahhanjan.** Hole and interstitial centres in radiation-resistant MgO single crystals. Tartu, 2008.
63. **Veera Krasnenko.** Computational modeling of fluorescent proteins. Tartu, 2008.
64. **Mait Müntel.** Detection of doubly charged higgs boson in the CMS detector. Tartu, 2008.
65. **Kalle Kepler.** Optimisation of patient doses and image quality in diagnostic radiology. Tartu, 2009.
66. **Jüri Raud.** Study of negative glow and positive column regions of capillary HF discharge. Tartu, 2009.
67. **Sven Lange.** Spectroscopic and phase-stabilisation properties of pure and rare-earth ions activated ZrO₂ and HfO₂. Tartu, 2010.
68. **Aarne Kasikov.** Optical characterization of inhomogeneous thin films. Tartu, 2010.

69. **Heli Valtna-Lukner.** Superluminally propagating localized optical pulses. Tartu, 2010.
70. **Artjom Vargunin.** Stochastic and deterministic features of ordering in the systems with a phase transition. Tartu, 2010.
71. **Hannes Liivat.** Probing new physics in e^+e^- annihilations into heavy particles via spin orientation effects. Tartu, 2010.
72. **Tanel Mullari.** On the second order relativistic deviation equation and its applications. Tartu, 2010.
73. **Aleksandr Lissovski.** Pulsed high-pressure discharge in argon: spectroscopic diagnostics, modeling and development. Tartu, 2010.
74. **Aile Tamm.** Atomic layer deposition of high-permittivity insulators from cyclopentadienyl-based precursors. Tartu, 2010.
75. **Janek Uin.** Electrical separation for generating standard aerosols in a wide particle size range. Tartu, 2011.
76. **Svetlana Ganina.** Hajusandmetega ülesanded kui üks võimalus füüsika-õppe efektiivsuse tõstmiseks. Tartu, 2011
77. **Joel Kuusk.** Measurement of top-of-canopy spectral reflectance of forests for developing vegetation radiative transfer models. Tartu, 2011.
78. **Raul Rammula.** Atomic layer deposition of HfO_2 – nucleation, growth and structure development of thin films. Tartu, 2011.
79. **Сергей Наконечный.** Исследование электронно-дырочных и интерстициал-вакансионных процессов в монокристаллах MgO и LiF методами термоактивационной спектроскопии. Тарту, 2011.
80. **Niina Voropajeva.** Elementary excitations near the boundary of a strongly correlated crystal. Tartu, 2011.
81. **Martin Timusk.** Development and characterization of hybrid electro-optical materials. Tartu, 2012, 106 p.
82. **Merle Lust.** Assessment of dose components to Estonian population. Tartu, 2012, 84 p.
83. **Karl Kruusamäe.** Deformation-dependent electrode impedance of ionic electromechanically active polymers. Tartu, 2012, 128 p.
84. **Liis Rebane.** Measurement of the $W \rightarrow \tau\nu$ cross section and a search for a doubly charged Higgs boson decaying to τ -leptons with the CMS detector. Tartu, 2012, 156 p.